DTIC FILE COPY

AFOSR-TR- 90 1037

(2)

AD-A226 895

Pseudomorphic InGaAs Materials

DTIC
ELECTE
SEP 27 1990
S E D

AFOSR
Final Technical Report
Air Force Contract No. F49620-88-C-0054

August 1990

Prepared for
Air Force Office of Scientific Research
Air Force Systems Command
Bolling Air Force Base
Washington, DC 20332-6448

Prepared by
GE Electronics Laboratory
PO Box 4840
Syracuse, NY 13221

DISTRIBUTION STATEMENT A
Approved for public release;
Distribution Unlimited

90 09 25 0[illegible]3

SECURITY CLASSIFICATION OF THIS PAGE

REPORT DOCUMENTATION PAGE

Form Approved OMB No. 0704-0188

1a. REPORT SECURITY CLASSIFICATION: Unclassified	1b. RESTRICTIVE MARKINGS
2a. SECURITY CLASSIFICATION AUTHORITY	3. DISTRIBUTION/AVAILABILITY OF REPORT: Approv[illegible] release; distribution unlimited.
2b. DECLASSIFICATION / DOWNGRADING SCHEDULE	
4. PERFORMING ORGANIZATION REPORT NUMBER(S)	5. MONITORING ORGANIZATION REPORT NUMBER(S)
6a. NAME OF PERFORMING ORGANIZATION: General Electric Electronics Laboratory; 6b. OFFICE SYMBOL (If applicable)	7a. NAME OF MONITORING ORGANIZATION: Air Force Office of Scientific Research
6c. ADDRESS (City, State, and ZIP Code): Electronics Park, Building 3, Syracuse, NY 13221	7b. ADDRESS (City, State, and ZIP Code): Building 410, Bolling Air Force Base, DC 20332-6448
8a. NAME OF FUNDING/SPONSORING ORGANIZATION: Air Force Office of Scientific Research; 8b. OFFICE SYMBOL (If applicable): NE	9. PROCUREMENT INSTRUMENT IDENTIFICATION NUMBER: F49620-88-C-0054
8c. ADDRESS (City, State, and ZIP Code): Building 410, Bolling Air Force Base, DC 20332-6448	10. SOURCE OF FUNDING NUMBERS: PROGRAM ELEMENT NO. 61102F; PROJECT NO. 2305; TASK NO C1; WORK UNIT ACCESSION NO.

11. TITLE (Include Security Classification): Pseudomorphic InGaAs Materials

12. PERSONAL AUTHOR(S): J.M. Ballingall, P. Ho, P. Martin, T. Yu

13a. TYPE OF REPORT	13b. TIME COVERED	14. DATE OF REPORT (Year, Month, Day)	15. PAGE COUNT
Final Technical	FROM Mar. 88 TO July 90	July 31, 1990	

16. SUPPLEMENTARY NOTATION

17. COSATI CODES			18. SUBJECT TERMS (Continue on reverse if necessary and identify by block number)
FIELD	GROUP	SUB-GROUP	Epitaxy, ~~AlGaAs-InGaAs-GaAs,~~ pseudomorphic heterostructures, strained layer superlattices, dislocations, photoluminescence, Hall effect, electron diffraction, photoreflectance.

19. ABSTRACT (Continue on reverse if necessary and identify by block number)

The objective of this program is to evaluate the dependence of pseudomorphic $In_xGa_{1-x}As$ quality on epitaxial growth conditions and $In_xGa_{1-x}As$ composition. All of the structures were fabricated by molecular beam epitaxy (MBE). The effects of different growth conditions were evaluated with a combination of characterization techniques, including Hall effect, Shubnikov-de Hass, photoreflectance, microwave reflectance, photoluminescence, transmission electron microscopy (TEM), and in-situ reflection high energy electron diffraction (RHEED). Critical layer thickness is shown to be a function of MBE growth temperature. Also, the interruption of $In_xGa_{1-x}As$ growth with a few monolayers of GaAs is shown to smoothen the $In_xGa_{1-x}As$ surface to provide strain relief, substantially extending the critical layer thickness. Modulation enhanced epitaxy is demonstrated to yield high quality pseudomorphic structures at temperatures as low as 300°C. Extensive materials characterization and modeling were applied to the structures, and excellent agreement was often obtained without resorting to adjustable parameters. Research progress on this contract enabled the development of $In_{0.35}Ga_{0.65}As$ single quantum well HEMTs which exhibited the best 18 and 60 GHz performance of any GaAs-based transistor. This work has led directly to 9 publications (4 in print, 5 in preparation) and 4 conference presentations, including one invited presentation.

20. DISTRIBUTION/AVAILABILITY OF ABSTRACT: ☐ UNCLASSIFIED/UNLIMITED ☐ SAME AS RPT. ☐ DTIC USERS	21. ABSTRACT SECURITY CLASSIFICATION: UNCLASSIFIED
22a. NAME OF RESPONSIBLE INDIVIDUAL: Dr. Gerald Witt	22b. TELEPHONE (Include Area Code): (202) 767-4931; 22c. OFFICE SYMBOL: NE

DD Form 1473, JUN 86 *Previous editions are obsolete.* SECURITY CLASSIFICATION OF THIS PAGE

Table of Contents

I INTRODUCTION AND SUMMARY 1-1

II RESEARCH PROGRESS 2-1

- A. Extending the Critical Layer Thickness with Reduced Substrate Temperature 2-1
- B. Layer Stability and Device Reliability 2-8
- C. Extending the Critical Layer Thickness with GaAs Smoothening Layers 2-11
- D. Electron Mobility Correlation with $In_xGa_{1-x}As$ Roughness 2-18
- E. Photoluminescence Measurements and Modeling 2-25
- F. Shubnikov de-Hass Measurements and Modeling 2-27
- G. Photoreflectance Measurements and Franz-Keldysh Oscillations 2-33
- H. Microwave Reflectance Measurements 2-36
- I. References 2-39

III SUGGESTIONS FOR FUTURE WORK 3-1

IV PUBLICATIONS 4-1

V PRESENTATIONS 5-1

VI PROFESSIONAL RESEARCH PERSONNEL 6-1

Accession For
NTIS GRA&I ☒
DTIC TAB ☐
Unannounced ☐
Justification
By
Distribution/
Availability Codes
Dist | Avail and/or Special
A-1

I. INTRODUCTION AND SUMMARY

The objective of this program is to evaluate the dependence of pseudomorphic $In_xGa_{1-x}As$ quality on epitaxial growth conditions and $In_xGa_{1-x}As$ composition. All of the structures were fabricated by molecular beam epitaxy (MBE). The effects of different growth conditions were evaluated with a combination of characterization techniques.

Key results to emerge from this work relate to the influence of substrate temperature on pseudomorphic InGaAs quality through controlling the roughness of the growth front and the kinetics for dislocation nucleation/propagation. Contrary to earlier findings, we observed that the roughening of the growth front doesn't necessarily coincide with the onset of dislocations, and that electron mobility can be severely degraded in samples free of dislocations. We also showed that the roughness of the growth front and the degree of mobility degradation are influenced by the roughness of the substrate; i.e., the "threshold" layer thickness at which electronic properties are noticeably degraded is a function of the substrate roughness. Thin (15Å) GaAs layers were shown to effectively smoothen the growth front and extend the threshold and critical layer thicknesses.

Migration-enhanced epitaxy (MEE) performed in the MBE system, and thus designated MBE/MEE, was demonstrated to yield high quality pseudomorphic structures at temperatures as low as 300°C. The electrical and structural properties of low temperature (LT) $In_{0.3}Ga_{0.7}As$ grown by MBE and MBE/MEE were compared and shown to be somewhat similar to LT GaAs. Work is in progress with Prof. Gerard Mourou and Dr. John Whitaker at the University of Michigan to assess the performance of LT InGaAs for ultrafast optical devices.

Extensive materials characterization and theoretical modelling was applied to the structures and excellent agreement was often observed without resorting to adjustable parameters. Dr. Chris Tigges, Dr. Jim Schirber, and Dr. Ian Fritz of Sandia National Laboratories performed Shubnikov-de Hass measurements on modulation-doped pseudomorphic structures and accurately modelled the electron subband populations in both single quantum well and thin-strained

superlattice structures. Models developed at GE gave very good agreement with subband energies assessed by low temperature photoluminescence in a wide variety of structures.

Two very promising non-contacting and non-destructive characterization techniques were applied for the first time to modulation-doped pseudomorphic structures. Prof. Fred Pollak of Brooklyn College performed photoreflectance measurements and observed above band-gap Franz-Keldysh oscillations. The oscillation period in energy yields a measure of the internal electric field in the InGaAs. Prof. Ron Guttman and Prof. Pepe Borrego of Rensselaer Polytechnic Institute applied microwave reflectance to assess the electron mobility in modulation-doped pseudomorphic InGaAs. Very good agreement was seen with conventional contacting Hall effect measurements.

Research progress on this contract has enabled the development of a new class of strained layer heterostructures which we call thin strained superlattices (TSSL), and high electron mobility transistor (HEMT) structures with x=0.3 and x=0.35 $In_xGa_{1-x}As$ single quantum well active layers, which on separate device projects at GE, have advanced the state-of-the-art of GaAs-based transistors. The stability of these metastable structures was evaluated and shown to be sufficient for any foreseen device applications. Device reliability data completed on other GE programs is included in this report to complement the high temperature heat treatment studies performed in the present work.

II. RESEARCH PROGRESS

A. Extending the Critical Layer Thickness with Reduced Substrate Temperature

The understanding of this area is becoming much more clear than it was two years ago. At that time, there were wide discrepancies in the values of critical layer thickness reported for the GaAs-$In_xGa_{1-x}As$ pseudomorphic system. Epitaxial theory states that there is a critical thickness up to which a strained layer of constant lattice misfit can be grown and still maintain coherency with the underlying substrate. Above the critical thickness, the strain can no longer be accommodated elastically and misfit dislocations are generated. The reasons for the reported discrepancies in critical layer thickness are now clear, partly due to this work as well as the work of others in this field. Principally there are two reasons. First of all, it is now established that the critical thickness is a function of growth conditions. We have demonstrated that lower substrate temperatures promote larger critical thicknesses. The understanding of this is that the kinetic barriers for misfit dislocation formation require sufficient growth temperatures (or post-growth temperatures) to be overcome. It turns out that relatively small differences in growth temperature (±5%) can make significant differences in the dislocation content of these structures. The second reason for earlier discrepancies is that the different measurement techniques employed for detecting misfit dislocation density vary widely in their sensitivity.

In this work we have utilized four techniques for detecting misfit dislocations—in-situ reflection high energy electron diffraction (RHEED), Hall electron mobility, photoluminescence, and transmission electron microscopy (TEM). Perhaps all four could be used quantitatively for assessing dislocation densities, though we have relied only on plan view TEM for quantitative analysis. The TEM uses two beam diffracting conditions in bright field mode. This has a detection limit of $10^4 cm^{-2}$, several orders of magnitude below the equilibrium misfit dislocation density ($\sim 10^{11} cm^{-2}$) for typical pseudomorphic structures (2% misfit strain) completely strain relieved through misfit dislocations. 10^4 cm^{-2} appears also to be about 2 orders of magnitude below the density at which effects of dislocations would normally be observed by Hall effect or photolu-

minescence. (An exception to this is photoluminescence microscopy[1] which can detect misfit dislocations to a limit of ~10 cm^{-2} because of a large sampling area.)

Figure 1 is a plot of critical layer thickness for several pseudomorphic single quantum well structures grown at GE. The structures were grown by MBE on LEC GaAs (100) ±0.5° oriented substrates with an As_4 to group III beam equivalent pressure ratio of 15 and a nominal growth rate of 1µm/h. The solid line is the Matthews-Blakeslee curve for critical layer thickness (CLT) calculated assuming a "single-kink" failure mechanism, i.e., dislocation propagation along the lower interface of the strained layer, the failure mechanism for single quantum well structures. For reference, the dashed line is the Matthews-Blakeslee curve for CLT assuming a "double-kink" failure mechanism, i.e., dislocation propagation along both interfaces of a strained superlattice. At low substrate temperatures (~480°C) we obtain structures with no detectable dislocations, but with thicknesses substantially above the Matthews-Blakeslee single-kink CLT. However, at higher substrate temperatures (~500-540°C) we see excellent agreement with the single-kink curve. As mentioned previously, this is believed to be due to kinetic barriers to single-kink dislocation formation. Coincidentally, the low substrate temperature CLTs are predicted better with the double-kink curve, at least for $x<0.3$. The RHEED technique can be useful here. Whaley and Cohen[2] demonstrated that the onset of lattice relaxation through misfit dislocations was simultaneously accompanied by three-dimensional growth manifested as spots or chevrons on the RHEED pattern. Their data for $x=0.33$, some of our previous RHEED data for $x=0.25$[3], and our RHEED data on this contract for $x=0.2$ to 0.35 agrees excellently with the Matthews-Blakeslee single-kink curve at the higher substrate temperatures.

The lower limits of substrate temperature were investigated. Figure 2 shows a representative TEM cross-section of modulation-doped pseudomorphic structures with $In_{0.2}Ga_{0.8}As$ layers grown at 300°C by MBE and MBE/MEE. The As_4 to group III beam equivalent pressure ratio was 15 and the growth rates were nominally 1µm/h for the MBE and 50% of that for the MBE/MEE. In MBE/MEE the group III and group V beams are alternated atomic layer by atomic layer with no

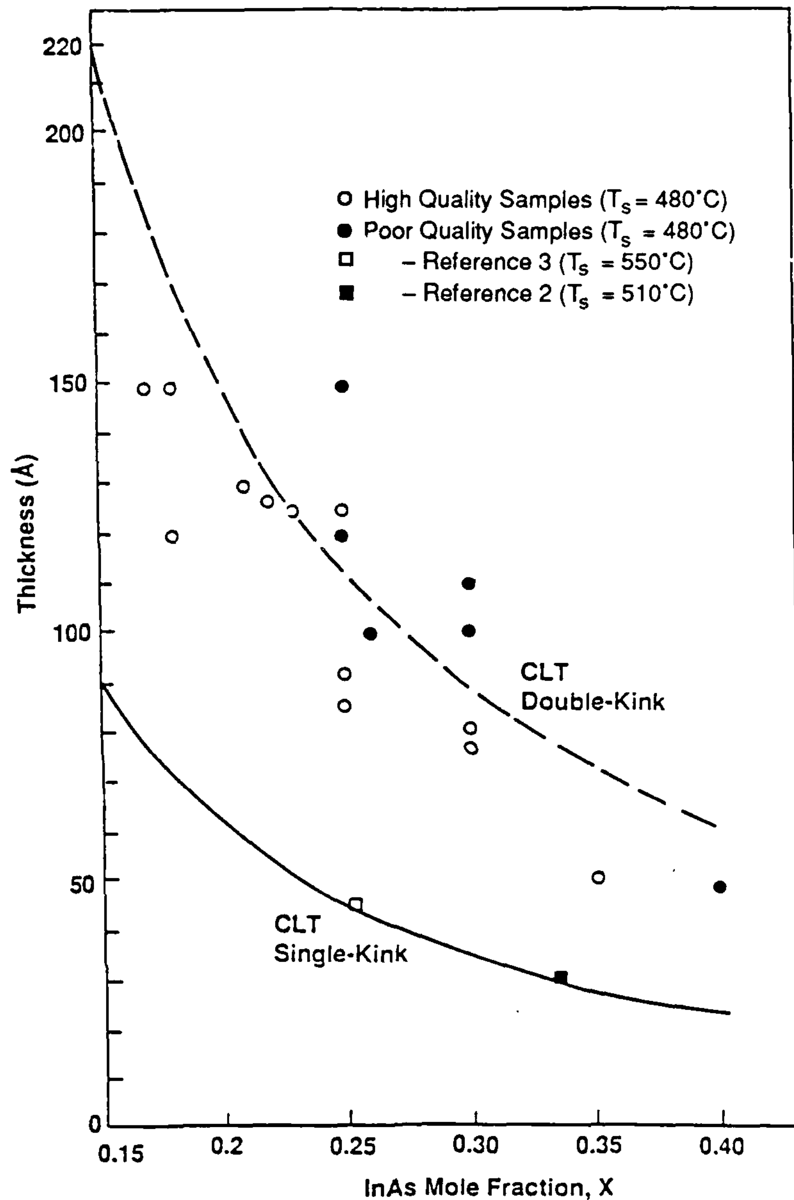

Figure 1. Critical Layer Thickness (CLT) for $In_xGa_{1-x}As$ on GaAs According to Matthews-Blakeslee Models for Single-kink and Double-kink Dislocation Mechanisms. Plotted circles are for modulation-doped single quantum well AlGaAs-$In_xGa_{1-x}As$-GaAs samples grown at GE by MBE at 480°C (o-samples with dislocation densities below 10^4 cm^{-2}, ●-samples with dislocation densities above 10^4 cm^{-2})

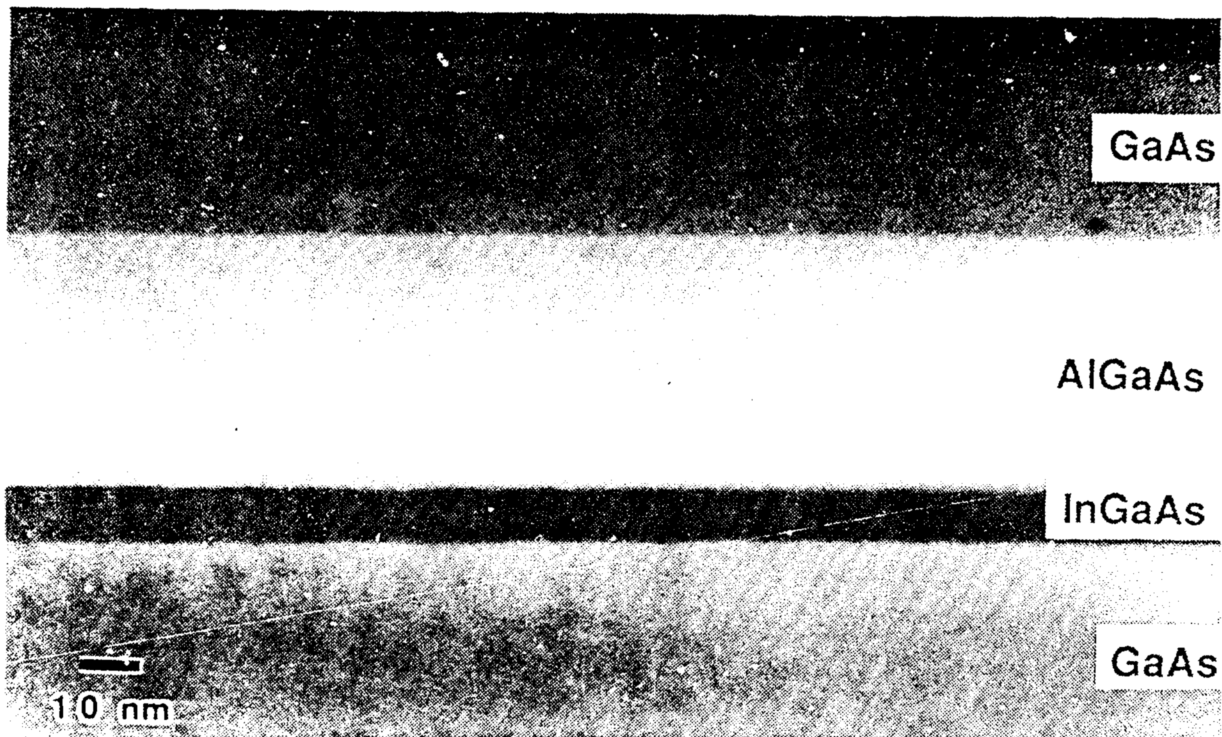

Figure 2. Representative Superlattice Dark-Field (110) TEM Cross-Section of MBE (3-1044) and MBE/MEE (3-1043) Pseudomorphic HEMT Structures with $In_{0.2}Ga_{0.8}As$ Layers Grown at 300°C

interruption between switching; thus, the group III beams are on 50% of the time relative to conventional MBE growth. The modulation doping was provided by silicon atomic planar doping at a concentration of $5x10^{12}$ cm^{-2} on top of a 45Å thick undoped $Al_{0.3}Ga_{0.7}As$ spacer layer. 400Å of Si-doped $Al_{0.3}Ga_{0.7}As$ and 350Å of Si-doped GaAs capped the structures as shown in Figure 2. The GaAs buffer layer and AlGaAs and GaAs overlayers were grown at 480°C by MBE. TEM cross sections of the MBE and MBE/MEE layers are indistinguishable, though the 77K electron mobility is substantially inferior for the MBE specimen (2800 cm^2/V-s versus 16,700 cm^2/V-s for the MBE/MEE sample). While the reduced growth rate is helpful, the key here is the enhanced cation moblity when the arsenic beam is switched off. The technique, in principle, could be exploited to achieve higher critical layer thicknesses, because of the low 300°C substrate temperature, but in practice the sample temperature needs to be elevated back above 450°C in order to get conducting GaAs and AlGaAs overlayers for modulation doping. Further development of MBE/MEE at low growth rates for the overlayers might lead to successful growth of the entire structure at 300°C.

Since no structural defects could be viewed in the thin (~100Å) 300°C InGaAs layers, thicker layers were grown. Figure 3 shows TEM plan view and cross-section micrographs of 1400Å thick $In_{0.3}Ga_{0.7}As$ layers grown at 300°C on GaAs substrates by MBE and MBE/MEE using the same growth conditions mentioned above. Both samples are similar in plan view and cross-section. A dislocation density on the order of 10^{10} cm^{-2} is apparent from the plan view micrographs, and the micrographs for the 300°C as-grown samples (2-1555, 2-1572) show no evidence of arsenic precipitates. Figure 4 shows cross-sections of the samples grown at 300°C and then heat treated at 600°C for ten minutes *in-situ* under an As_4 flux. Precipitates are clearly visible in both the MBE and MBE/MEE samples. Table 1 summarizes some of the Hall effect data taken on these four 300°C specimens. The electron mobility is superior for the heat-treated MBE/MEE specimen, correlating with the results for the modulation-doped structures. Generally, the structural and electrical data is similar to that of LT GaAs.[4-6] Because of the small size (20-60Å) of the precipitates and the strain of the samples, it wasn't possible to conclusively identify the particles as arsenic with high resolution imaging, as we have done with LT GaAs.[6] Prof. Gerard Mourou and Dr. John Whitaker at the University of Michigan are comparing these samples with LT GaAs as ultra-fast optical switches.

Table 1. 300°C $In_{0.3}Ga_{0.7}As$ Electrical Characterization Data

Sample	Growth	Post Growth Heat Treatment	300K Sheet Resistivity	300K Electron Sheet Density/Mobility
2-1555	MBE	None	$3x10^7$ Ω/□	$2.7x10^8$ cm^{-2} / 780 cm^2/V-s
2-1556	MBE	600°C/10 min.	$6x10^7$ Ω/□	$8x10^7$ cm^{-2} / 1300 cm^2/V-s
2-1572	MBE/MEE	None	$5x10^6$ Ω/□	$1.9x10^9$ cm^{-2} / 635 cm^2/V-s
2-1573	MBE/MEE	600°C/10 min.	$4x10^8$ Ω/□	$5.4x10^6$ cm^{-2} / 2900 cm^2/V-s

R-8/90-1AT

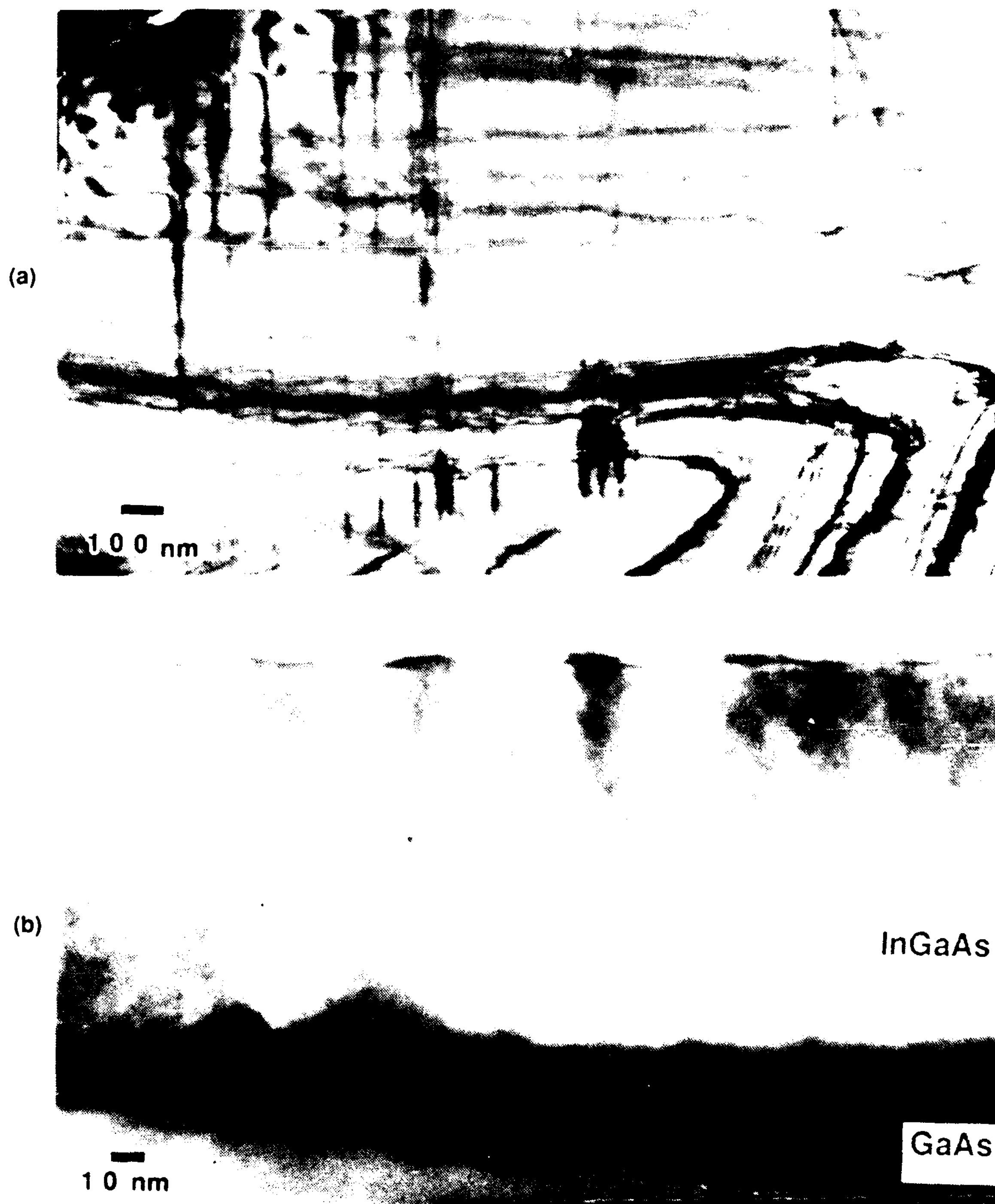

Figure 3. Representative TEM (a) bright field (100) plan view, and (b) dark field (110) cross-section of $In_{0.3}Ga_{0.7}As$ grown by MBE and MBE/MEE at 300°C

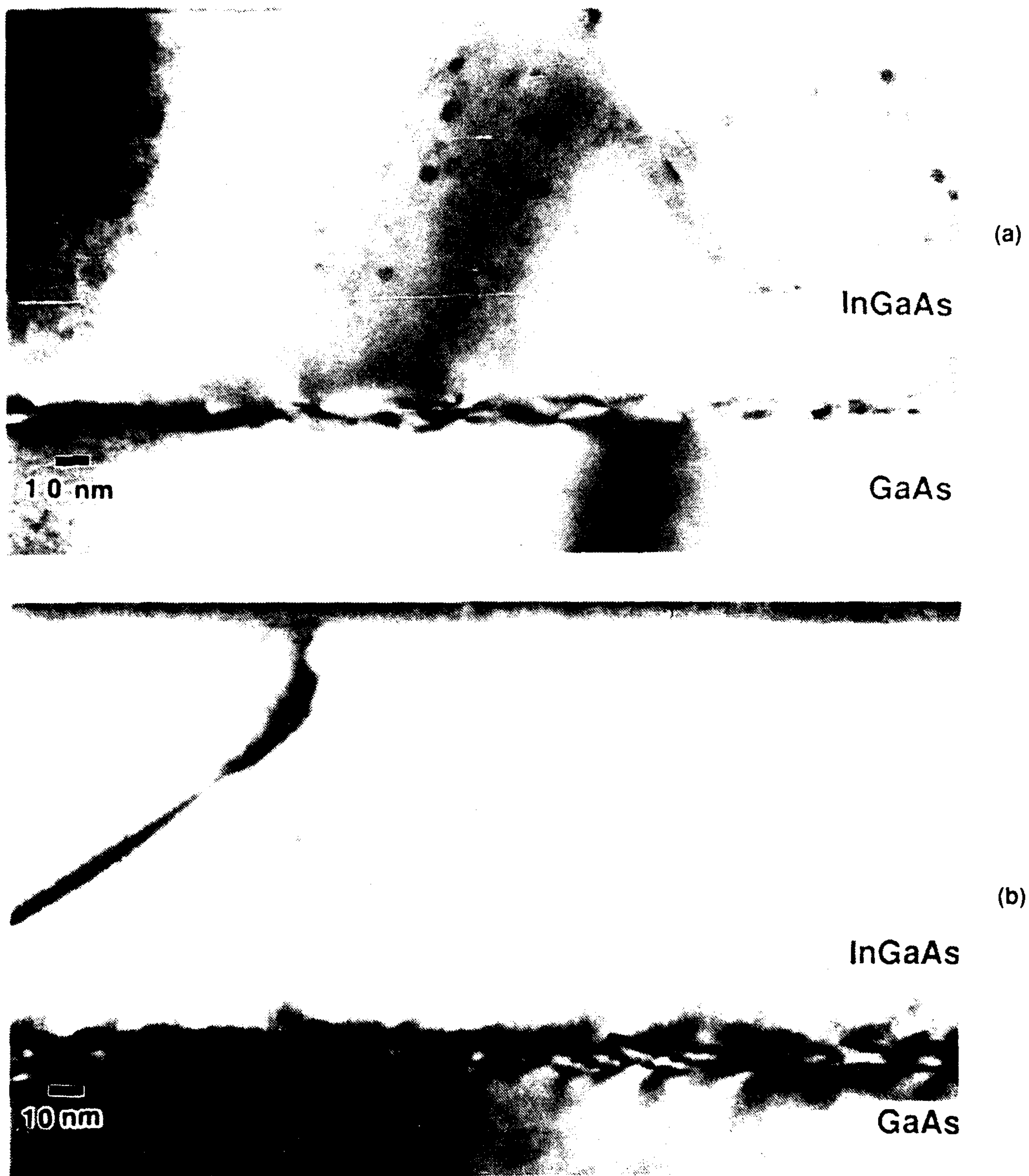

Figure 4. TEM Bright Field (110) cross-sections of $In_{0.3}Ga_{0.7}As$ grown at 300°C by (a) MBE (3-1556) and (b) MBE/MEE (3-1573) and then subjected to in-situ heat treatment at 600°C. Precipitates are clearly visible after heat treatment.

Table 2. Hall Effect Data for As-grown and Heat-Treated Pseudomorphic HEMT Structures

	X	W(Å)	Sheet Resistivity (300K) As-grown/Heat-treated	Electron Mobility, Sheet Density (77K)	
				As-grown	Heat-treated
2-1564	0.3	80	228/232 $\Omega/\square$	14,320 cm^2/V–s, $3.1x10^{12}$ cm^{-2}	11,790 cm^2/V–s, $3.1x10^{12}$ cm^{-2}
2-1570	0.3	80	226/279 $\Omega/\square$	15,890 cm^2/V–s, $2.8x10^{12}$ cm^{-2}	10,100 cm^2/V–s, $3.3x10^{12}$ cm^{-2}
2-1574	0.2	125	199/222 $\Omega/\square$	13,950 cm^2/V–s, $3.8x10^{12}$ cm^{-2}	9,950 cm^2/V–s, $3.3x10^{12}$ cm^{-2}

R-8/90-2AT

B. Layer Stability and Device Reliability

The stability of pseudomorphic structures was evaluated by comparing electron mobility and photoluminescence measurements before and after rapid thermal anneals (RTA) at 865°C for 5 seconds. This is the temperature/time RTA cycle employed to anneal GaAs ion implant damage at GE. As shown earlier,[7] heat treatment substantially above the growth temperature is expected to relieve the strain of metastable structures through the nucleation of misfit dislocations. The degradation in electron mobility observed in the four pseudomorphic structures annealed is evidence for dislocation formation, though clearly the results shown in Table 2 are not catastrophic. Results leave open the possibility that an acceptable RTA cycle might be developed which would remove implant damage, yet also have a minimal effect on the structural and electronic quality of metastable pseudomorphic structures. For device fabrication processes which do not require ion implantation, we have demonstrated that pseudomorphic HEMT reliability can be equivalent to conventional GaAs FETs.

Figure 5 shows pseudomorphic HEMT device median time to failure (MTF) estimates based on reliability tests conducted on other GE programs. The data is included here to complement the above RTA studies. Low noise devices were tested under DC bias at three temperatures (up to 250°C). If device failure is defined at 10% (or 20%) degradation in device transconductance,

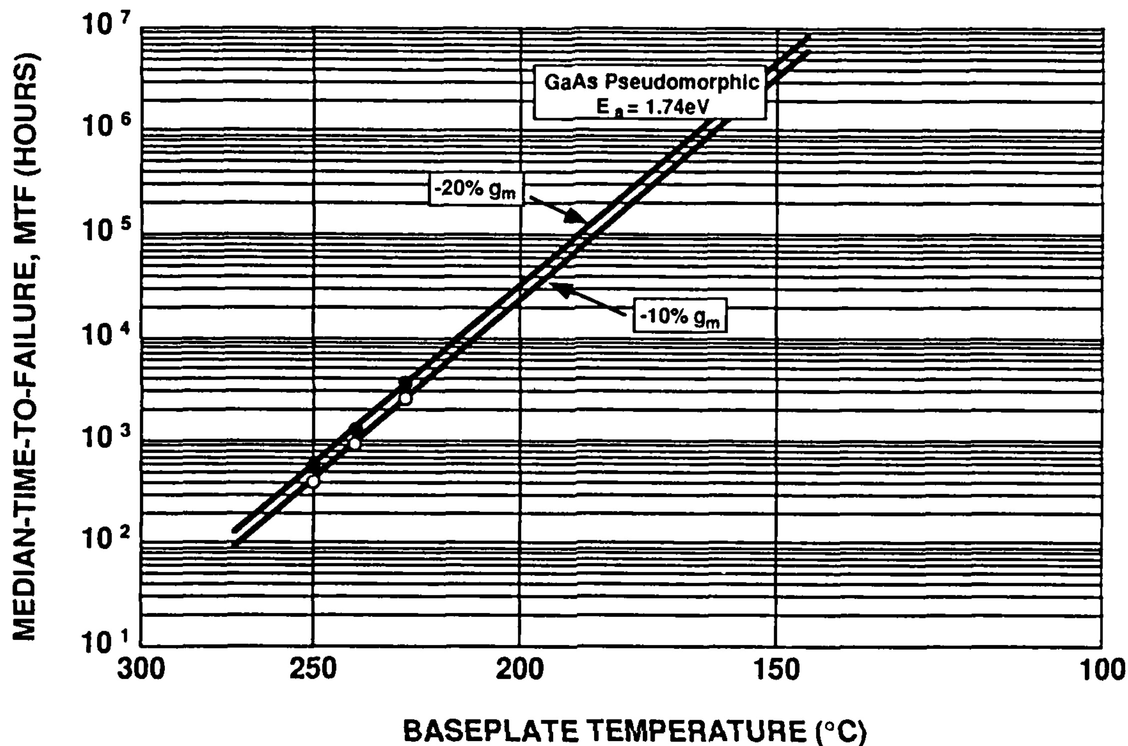

Figure 5. Measured and Extrapolated Median Time to Failures for Pseudomorphic HEMTs. Results indicate MTF comparable to GaAs FETs with degradation in transconductance, g_m, due to ohmic contact metallizations.

then an MTF of 2×10^6 (or 4×10^6) hours at 150°C is extrapolated. Low noise devices would normally have a base plate temperature below 100°C, and power devices would have a base plate temperature below 150°C. The MTF is comparable to GaAs FETs; and, in fact, the failure mechanism is a similar degradation in ohmic contact metallization. This result holds for devices with 80Å-thick $In_{0.3}Ga_{0.7}As$ single quantum wells and hasn't yet been tested at higher InAs mole fractions. The key to reliability for these metastable structures is that device fabrication temperatures are below the growth temperature of 480°C.

Figure 6 shows a TEM cross-section of a 50Å-thick $In_{0.35}Ga_{0.65}As$ single quantum well HEMT structure grown at 480°C. This is the highest InAs mole fraction fabricated in a pseudomorphic HEMT. Plan-view (100) bright-field TEM measurements of the layer detected no dislocations in

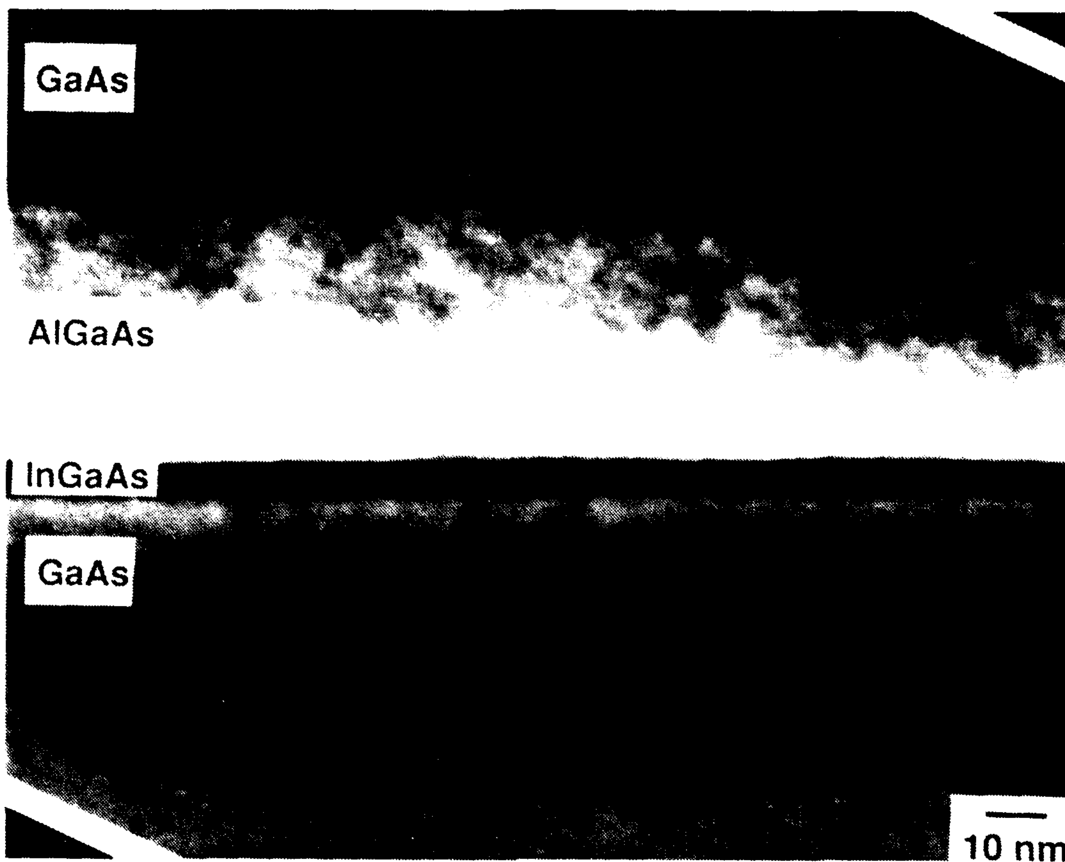

Figure 6. Cross-sectional (110) TEM Superlattice Dark-Field Image of $In_{0.35}Ga_{0.65}As$ HEMT Epitaxial Structure, Demonstrating Pseudomorphic Growth

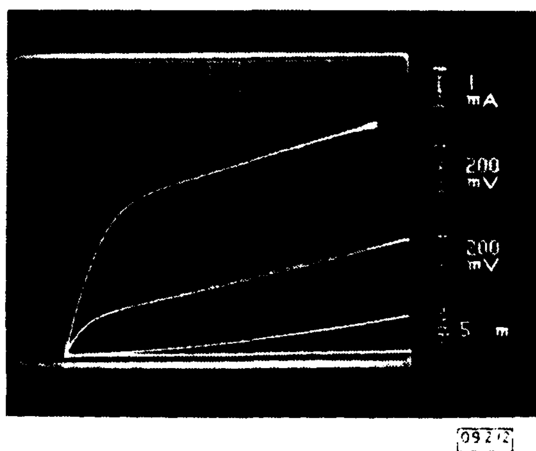

Figure 7. Drain I/V Characteristics of 0.15 μm x 30 μm $In_{0.35}Ga_{0.65}As$/GaAs Pseudomorphic HEMT. Top curve: V_{gs} = 0.2V. Device has maximum g_m of 700mS/mm at V_{ds} = 2V and V_{gs} = 0.1V.

this material down to the detection limit of 10^4 cm^{-2}. Hall measurements of this HEMT structure yielded a two dimensional electron gas sheet charge density of 3.2×10^{12} cm^{-2} with electron mobilities of 5000 and 11600 cm^2/V-s at room temperature and 77K, respectively. The Hall measurements were performed after removing the n^+-GaAs contact layer and part of the n-AlGaAs gate barrier layer to minimize parallel conduction with the two-dimensional electron gas. Figure 7 shows the drain I/V characteristic of the 0.15μm gate length device, which exhibits an extrinsic transconductance of 700 mS/mm. At 18 GHz, the device yields 0.55 dB noise figure with 15.0 dB associated gain. At 60 GHz, the device yields 1.6 dB noise figure with 7.6 dB associated gain. This is the best performance yet reported for a GaAs-based transistor.[8]

In addition to the effects of substrate temperature on critical layer thickness, we've discovered in the course of this work that a new structure known as the thin strained superlattice enables the growth of pseudomorphic structures substantially above the critical layer thickness for single quantum wells grown at the same temperature. This success is related to surface smoothening of the growth front and strain relief. The results are discussed in the next section.

C. Extending the Critical Layer Thickness with GaAs Smoothening Layers

The lattice mismatch strain between $In_xGa_{1-x}As$ and GaAs has generally precluded the use of $In_xGa_{1-x}As$ with x>0.3 for what are essentially two distinct issues. First of all, the mismatch strain imposes quantum well thicknesses which are often too thin for practical devices. The relationship between the $In_xGa_{1-x}As$ critical layer thickness (CLT) and InAs mole fraction x demands that high x pseudomorphic layers have critical thicknesses so thin that quantum size effects push electron subband energy levels up, substantially reducing the electron confinement potential which would be realized with bulk materials or thick quantum wells. Also for thin wells a larger fraction of the electron wave function penetrates more deeply into the AlGaAs barrier layers enhancing the scattering rate. The second issue is that the high x materials, having a lattice mismatch with GaAs greater than 2%, are difficult to grow with high electronic quality. Problems with the crystal growth manifested as surface roughening, three-dimensional growth,

and islanding appear to limit the electronic quality of high x layers[9], even with thicknesses comparable to or less than the CLT.[10]

In this section we present results for a new class of pseudomorphic HEMT structures which utilize thin strained superlattice (TSSL) active layers as opposed to the conventional single quantum wells (SQW). These new active layers provide a means for enhancing the InAs mole fraction content of HEMT active layers by simultaneously addressing both of the mismatch strain-related issues mentioned above. A typical TSSL HEMT active layer is shown in Figure 8, with three periods of GaAs(15Å)-$In0_{3}Ga_{0.7}As$(52Å). The idea is two-fold. First of all, the GaAs layers are sufficiently thin to be relatively transparent to the electrons such that the TSSL contains one two-dimensional electron gas (2-DEG) with a low energy ground state as opposed to three 2-DEGs with considerably higher energy ground states. This enhances the effective conduction band discontinuity compared to a single quantum well or a multi-quantum well with thick GaAs layers. Secondly, the GaAs layers are sufficiently thick to provide strain relief and surface smoothening of the $In_xGa_{1-x}As$ to alleviate the problems mentioned above with the crystal growth.

Pseudomorphic HEMT structures were grown by MBE on LEC GaAs (100) ±0.5° oriented substrates. The substrate temperature was 480°C±10°C for all of the layers with an As_4 to group III beam equivalent pressure ratio of 15 and a nominal growth rate of 1μm/h. The modulation doping was provided by silicon atomic planar-doping at a concentration of $5x10^{12}cm^{-2}$ on top of a 45Å thick undoped $Al_{0.3}Ga_{0.7}As$ spacer layer. 400Å of Si-doped $Al_{0.3}Ga_{0.7}As$ and 350Å of Si-doped GaAs capped the structures as shown in Figure 8. The layers were characterized by Hall effect, Shubnikov-de Hass (SdH), photoluminescence, and transmission electron microscopy. All Hall samples were differentially etched to the point of maximizing the measured 77K mobility, in order to minimize the effects of parallel conduction in the doped GaAs and AlGaAs layers. This method gave excellent agreement with SdH densities. TEM measurements were performed on cross-sectional samples utilizing both bright-field and dark-field imaging modes. Plan view

(a)

Layer	Thickness	Doping	
GaAs	350Å	Si-DOPED	
$Al_{0.3}Ga_{0.7}As$	400Å	Si-DOPED	
$Al_{0.3}Ga_{0.7}As$	45Å	UNDOPED	SPACER LAYER
$In_xGa_{1-x}As$	h(Å)	UNDOPED	} Active Layer
GaAs Buffer Layer	1µm	UNDOPED	
GaAs Substrate			

(b)

Layer	Thickness	Doping	
GaAs	350Å	Si-DOPED	
$Al_{0.3}Ga_{0.7}As$	400Å	Si-DOPED	
$Al_{0.3}Ga_{0.7}As$	45Å	UNDOPED	SPACER LAYER
$In_xGa_{1-x}As$	h_2(Å)	UNDOPED	Active Layer
GaAs	h_1(Å)	UNDOPED	Active Layer
$In_xGa_{1-x}As$	h_2(Å)	UNDOPED	Active Layer
GaAs	h_1(Å)	UNDOPED	Active Layer
$In_xGa_{1-x}As$	h_2(Å)	UNDOPED	Active Layer
GaAs Buffer Layer	1µm	UNDOPED	
GaAs Substrate			

Figure 8. Cross-section Schematic of Modulation-Doped Pseudomorphic $In_xGa_{1-x}As$ Structures with (a) Single Quantum Well and (b) Thin Strained Superlattice Active Layers

Table 3. Electrical Data for Modulation-Doped Pseudomorphic Structures

$In_{0.3}Ga_{0.7}As$ Single Quantum Wells (SQW)

SQW Thickness (Å)	77K Mobility (cm^2/V-s)	77K Sheet Density (cm^{-2})
40	13,800	$2.4x10^{12}$
80	14,400	$2.8x10^{12}$
100	700	$3.4x10^{12}$

$GaAs(h_1)-In_{0.3}Ga_{0.7}As(h_2)$ Thin Strained Superlattices (TSSL)

h_1/h_2 (Å)	TSSL Thickness (Å)	77K Mobility (cm^2/V-s)	77K Sheet Density (cm^{-2})
15/30	135	12,700	$2.5x10^{12}$
15/42	171	10,300	$2.6x10^{12}$
15/52	201	9,200	$3.0x10^{12}$

R-8/90-3AT

imaging utilized two-beam diffracting conditions in bright-field mode for assessing dislocation densities.

Table 3 shows the effect of layer thickness on electron mobility and sheet density for $In_{0.3}Ga_{0.7}As$ SQWs and $GaAs-In_{0.3}Ga_{0.7}As$ TSSLs. For SQWs the electron mobility is substantially degraded for x=0.3 layers thicker than 80-100Å. Plan-view TEM investigation of the 100Å thick SQW showed a dislocation density of $10^{10}cm^{-2}$, which is obviously responsible for the dramatic degradation in electron mobility compared to the thinner SQWs. The TSSLs, on the other hand, show a more gradual and less severe degradation in electron mobility; for a total $In_{0.3}Ga_{0.7}As$ thickness of 156Å and a total TSSL thickness of 201Å, the electronic parameters are still quite acceptable.

Figure 9 shows a cross-sectional TEM superlattice bright field image of the thickest TSSL listed in Table 3 and shown schematically in Figure 8. Only one misfit dislocation was seen in all of the cross-sectional areas examined, and this dislocation occurred at the interface between

(a)

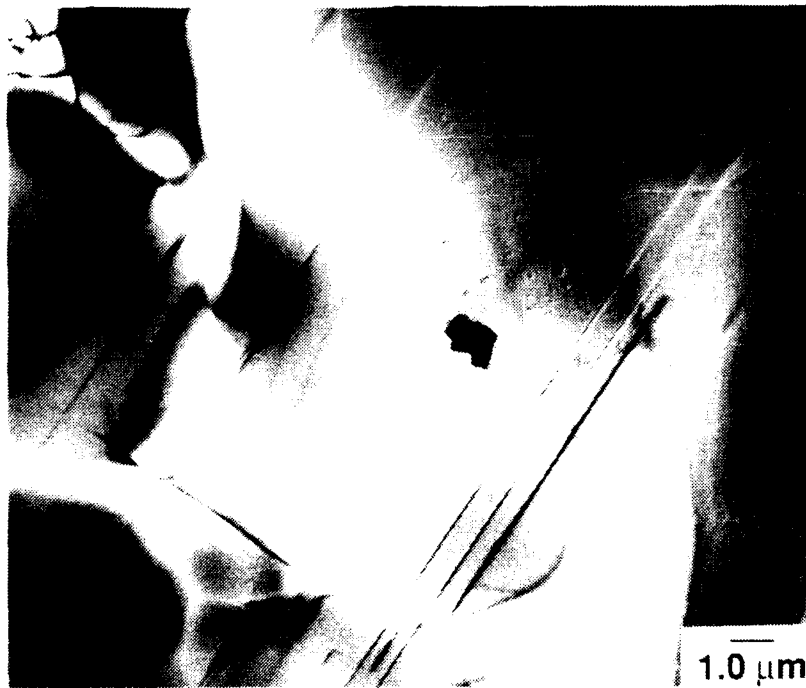

(b)

Figure 9. (a) Cross-sectional (110) TEM of TSSL Shown Schematically in Figure 8, Demonstrating Pseudomorphic Growth (Superlattice Bright Field Imaging Mode); (b) Plan-view (100) Bright Field Transmission Electron Micrograph of the Above TSSL Showing Linear Misfit Dislocations Which Lie Along <110>. Bend Contours (Wavy Lines) Are Also Visible. Dislocation Density in This Sample is 10^6 cm^{-2}. No Dislocations Were Detected in the Thinner TSSLs Down to a Detection Limit of 10^4 cm^{-2}.

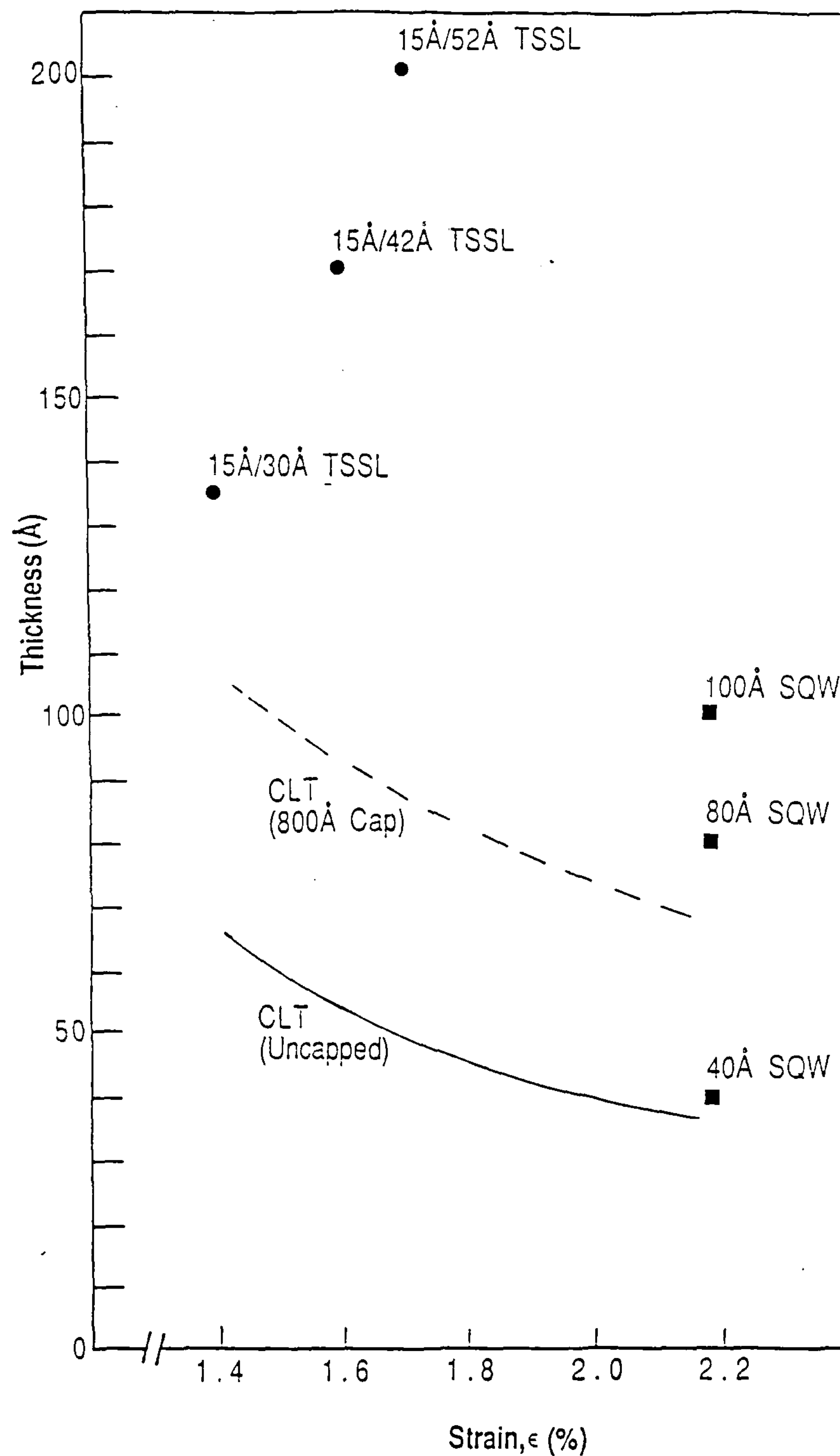

Figure 10. Plots of Layer Thickness vs. Strain for SQWs and TSSLs Listed in Table 3. Solid and dashed lines are theoretical critical layer thicknesses (CLT) for, respectively, an uncapped strained layer and a strained layer with an 800Å-thick unstrained capping layer. Both curves assume the single-kink failure mechanism.

the GaAs buffer layer and the first InGaAs layer. Plan-view TEM such as shown in Figure 9 confirmed a misfit dislocation density of 10^6 cm^{-2} in this sample. Plan-view TEM of the thinner TSSLs detected no dislocations down to a detection limit of 10^4 cm^{-2}.

Figure 10 shows two plots of critical layer thickness versus strain calculated using the concepts developed recently concerning the stability and metastability for buried strained layers.[7] Critical layer thicknesses are calculated for the "single-kink" failure mechanism, i.e., dislocation propagation along the lower interface of the strained layer, for (1) an uncapped strained layer and (2) a strained layer capped with an 800Å-thick unstrained layer. Good agreement is observed, as mentioned in Section A, between the uncapped CLT curve of Figure 10 and temperature dependent in-situ reflection high energy electron diffraction (RHEED) measurements when the substrate temperatures are sufficiently high to apparently circumvent kinetic barriers to dislocation formation. These results, in fact, led us to utilize the relatively lower substrate temperature of 480°C for this work. The total thickness of the strained layers of Table 3 is also plotted in Figure 10 versus their strain. To calculate the strain for the TSSLs, we utilized the "free-standing" lattice constant of the TSSL, i.e. we treat the TSSL as if it has an in-plane lattice constant given by the following expression,[11]

$$a = a_1 \left\{ 1 + \left(\frac{(a_2 - a_1)/a_1}{1 + (G_1 h_1 / G_2 h_2)} \right) \right\} \quad (1)$$

where a_1 and a_2 are the lattice constants for GaAs and $In_xGa_{1-x}As$, respectively, h_1 and h_2 are the thicknesses of the GaAs and $In_xGa_{1-x}As$ layers forming each period for the TSSL, and G_1 and G_2 are the respective shear moduli for each material (assumed equal for these structures). All of the layers, except for the 40Å SQW, have thicknesses exceeding the CLT for strained layers with an 800Å unstrained capping layer, and so like most pseudomorphic HEMT structures, are predicted to be metastable. Thus, the TSSLs would be expected to degrade with high temperature processing such as post-implant annealing, as demonstrated for SQW samples in Section B, but other-

wise could be expected to be long-lived because of the sluggish kinetics for dislocation formation.[7] It is not clear why the TSSLs can be grown to thicknesses which exceed their respective CLTs more than the SQWs; though strain, being the driving force for dislocation formation and perhaps as well for changes in growth kinetics[12] independent of dislocation formation, is significantly reduced and assumed to be the key factor.

Several authors have reported the continual diminishing of the *in-situ* RHEED intensity with the growth of pseudomorphic $In_xGa_{1-x}As$[2,13,14]. For GaAs-$In_xGa_{1-x}As$-GaAs double heterostructures, it was noted that the decrease in RHEED intensity which occurred during the $In_xGa_{1-x}As$ layer was followed by a substantial recovery in intensity during the GaAs overlayer, an effect which the authors related to three-dimensional growth.[14] We find that the RHEED intensity generally recovers to 70-90% of its starting intensity after only 5 monolayers of GaAs on $In_xGa_{1-x}As$. When the In beam is recommenced for the successive $In_xGa_{1-x}As$ layer, the intensity again diminishes, but then later recovers with the following GaAs layer. Thus, for TSSL growth, the RHEED intensity exhibits periodic oscillations with the superlattice period, which form an envelope for the monolayer oscillations as shown in Figure 11. Very similar behavior has been reported for GaAs-AlAs short period superlattices and attributed to surface roughening by the AlAs layers alternated with smoothening by the GaAs layers.[15] Contrary to the results quoted above for double heterostructures[14], we did not observe any three-dimensional features (e.g., spots or chevrons) on the RHEED patterns of the TSSLs, and so favor an interpretation here based simply on surface smoothening by the GaAs layers. The lack of three-dimensional features on the RHEED pattern for the TSSLs is in agreement with the temperature dependent RHEED studies cited earlier.[2,3]

D. Electron Mobility Correlation with $In_xGa_{1-x}As$ Roughness

After succeeding with the x=0.3 TSSLs, we began development of x=0.35 and x=0.4 TSSLs. Table 4 lists the structural parameters (composition and thickness) with the Hall mobilities for some of those layers. Three period superlattices for x=0.35 had rather low electron mobilities, so

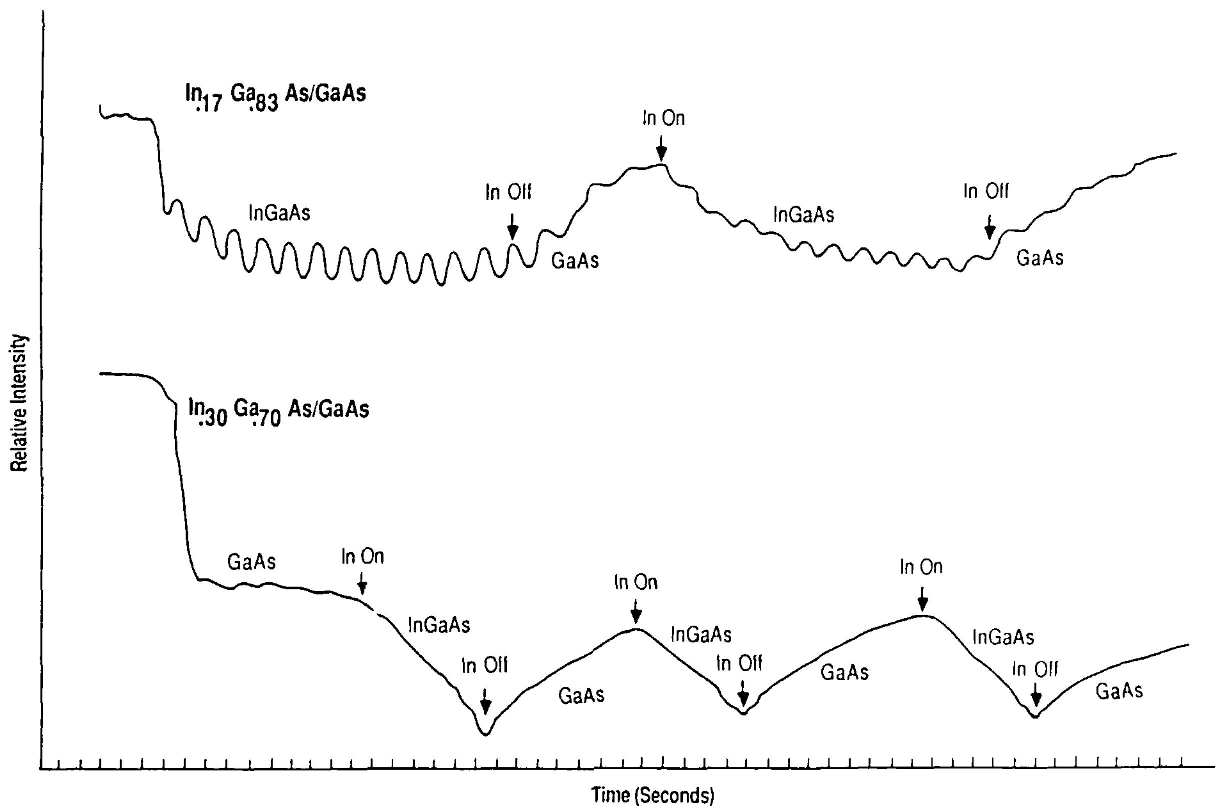

Figure 11. In-situ RHEED Intensity Oscillations for $In_xGa_{1-x}As$-GaAs TSSLs Showing Intensity Recovery with Deposition of Thin GaAs Layers

Table 4. Electrical Data for Modulation-Doped GaAs(h_1)-$In_xGa_{1-x}As$(h_2) TSSLs and $In_xGa_{1-x}As$ SQWs

Sample	X	h_1/h_2 (Å)	No. of Periods	77K Mobility (cm^2/V-s)	77K Sheet Density (cm^{-2})	MD Density (cm^{-2})
3-443	0.25	15/30	3	15,000	3.0×10^{12}	ND*
3-448	0.30	15/30	3	12,700	2.5×10^{12}	ND
3-449	0.30	15/42	3	10,300	2.6×10^{12}	ND
3-450	0.30	15/52	3	9,200	3.0×10^{12}	10^6
3-533	0.30	15/62	2	12,700	2.8×10^{12}	10^5
3-452	0.35	15/30	3	2,500	2.6×10^{12}	ND
3-535	0.35	15/32	2	11,800	2.5×10^{12}	ND
3-663	0.35	15/40	2	4,100	2.9×10^{12}	ND
3-668	0.40	15/25	2	8,800	2.8×10^{12}	ND
3-664	0.40	15/34	2	1,100	3.7×10^{12}	ND
3-451	0.30	78	SQW	14,500	3.0×10^{12}	ND
3-532	0.30	80	SQW	14,400	2.8×10^{12}	ND
3-534	0.35	50	SQW	11,600	3.2×10^{12}	ND
3-665	0.40	48	SQW	940	5.7×10^{12}	ND

R-8/90-4AT

*None detected

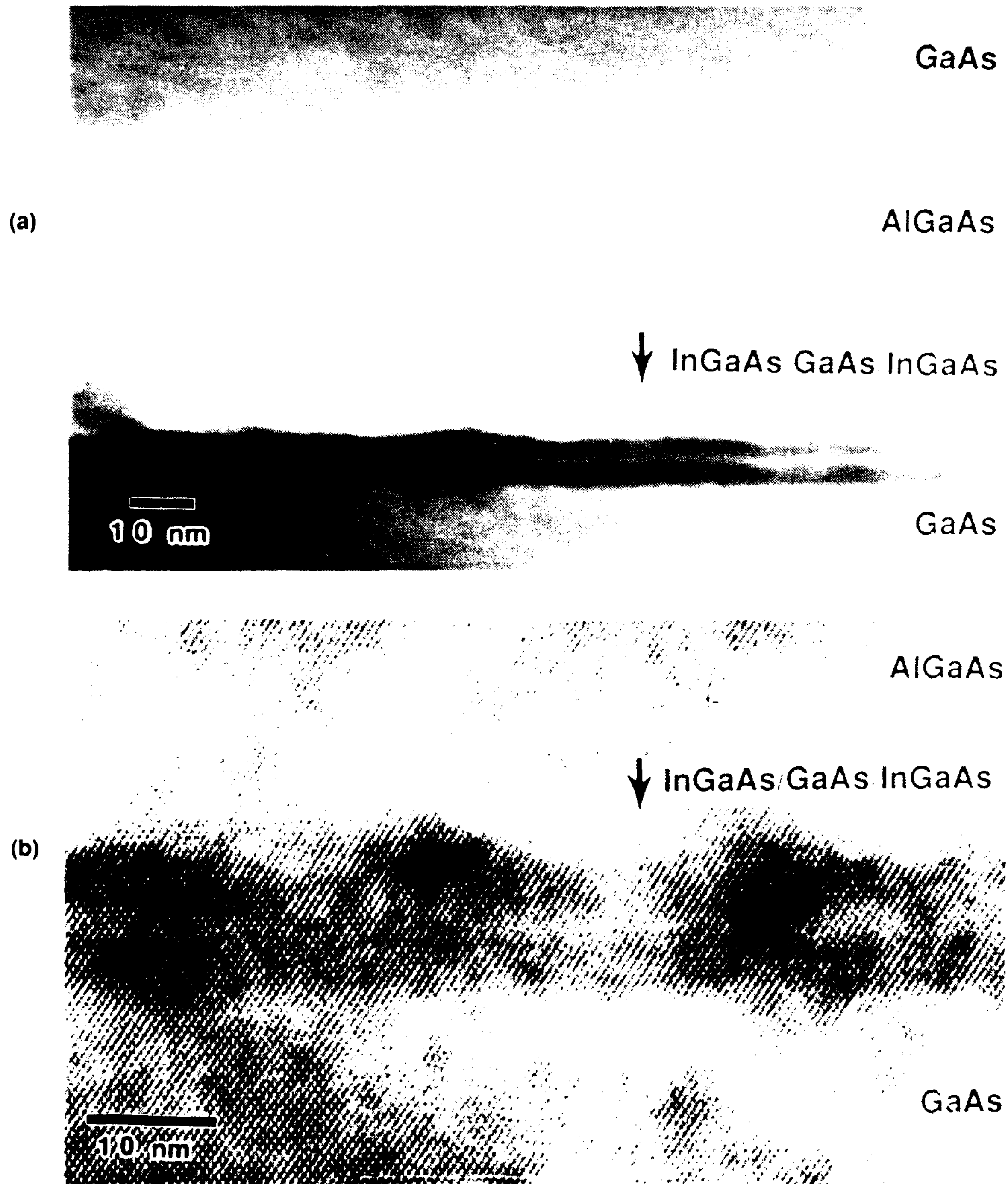

Figure 12. (a) Cross-sectional (110) Superlattice Dark Field TEM Image of a GaAs (15Å)-$In_{0.4}Ga_{0.6}As$(25Å), Two Period TSSL. (b) Cross-sectional (110) High Resolution TEM Image of Same Specimen (3-668).

we investigated two period TSSLs for x=0.35 and x=0.4. The degradation in electron mobility correlates with the detection of dislocations by TEM (measured using planar samples) for x=0.3 SQWs and TSSLs. However, we did not see such a correlation for x=0.35-0.4, though the cross-sectional TEM does indicate surface roughening in all of the samples with degraded mobility. For example, Figure 12 shows cross-sectional TEM photos in dark field and high resolution modes of the x=0.4 TSSL listed in Table 4 which exhibited a mobility of 8800 cm^2/V-s. The wavy interface contrast viewed in the dark field images (Figure 12a) initially suggested the presence of "strain centers" (defects which contribute strain) along the top InGaAs interface. Plan-view and high resolution TEM (Figure 12b) was subsequently performed on several other samples from this wafer, as well as the x=0.4 SQW with a mobility of 940 cm^2/V-s. None of these images showed defects or dislocations at the InGaAs interfaces. Thus from this data, we feel that the apparent roughness is not due to strain centers and is not a measurement artifact, but is indicative of a change in growth kinetics in the most highly strained films.

Figures 13 and 14 show the progression of this roughness for increasing $In_xGa_{1-x}As$ thickness and InAs mole fraction. The correlation with mobility degradation can be followed from Table 4. The full width at half maximum for photoluminescence (PL) measurements also correlated with the roughness and mobility degradation. The PL data is presented in the next section.

Figure 15 shows an interesting correlation between the roughness of the underlying AlGaAs and the roughness of the InGaAs and the electron mobility in the InGaAs. AlGaAs roughness is controlled by the AlGaAs growth temperature, higher temperatures lead to smoother AlGaAs, with 680°C-700°C giving surfaces somewhat comparable to 600°C GaAs. Sample 3-872 has a GaAs-AlGaAs superlattice buffer grown at 680°C, while 3-873 has a superlattice buffer grown at 520°C. Both layers have a 125Å-thick $In_{0.22}Ga_{0.78}As$ quantum well grown at 480°C. The 77K electron mobility is reduced from 12,600 cm^2/V-s to 5200 cm^2/V-s. Thus, the quality of the starting substrate has a strong effect on the "threshold" thickness at which roughening of the

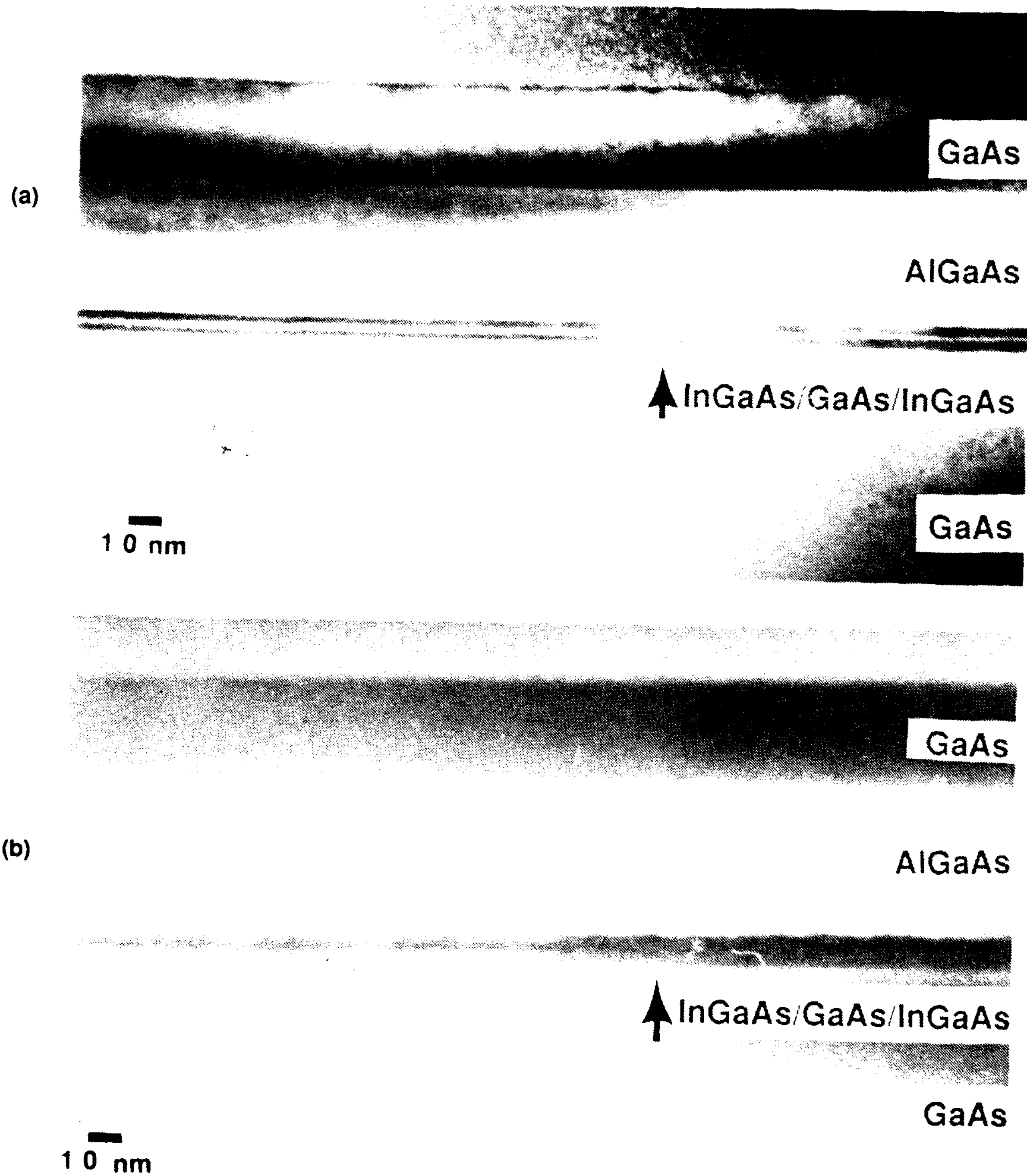

Figure 13. Superlattice Dark Field (110) TEM Cross-sections of x=0.35 TSSLs with h_1=15Å and (a) h_2=32Å (3-535), and (b) h_2=40Å(3-663). Roughening is evident in the thicker TSSL.

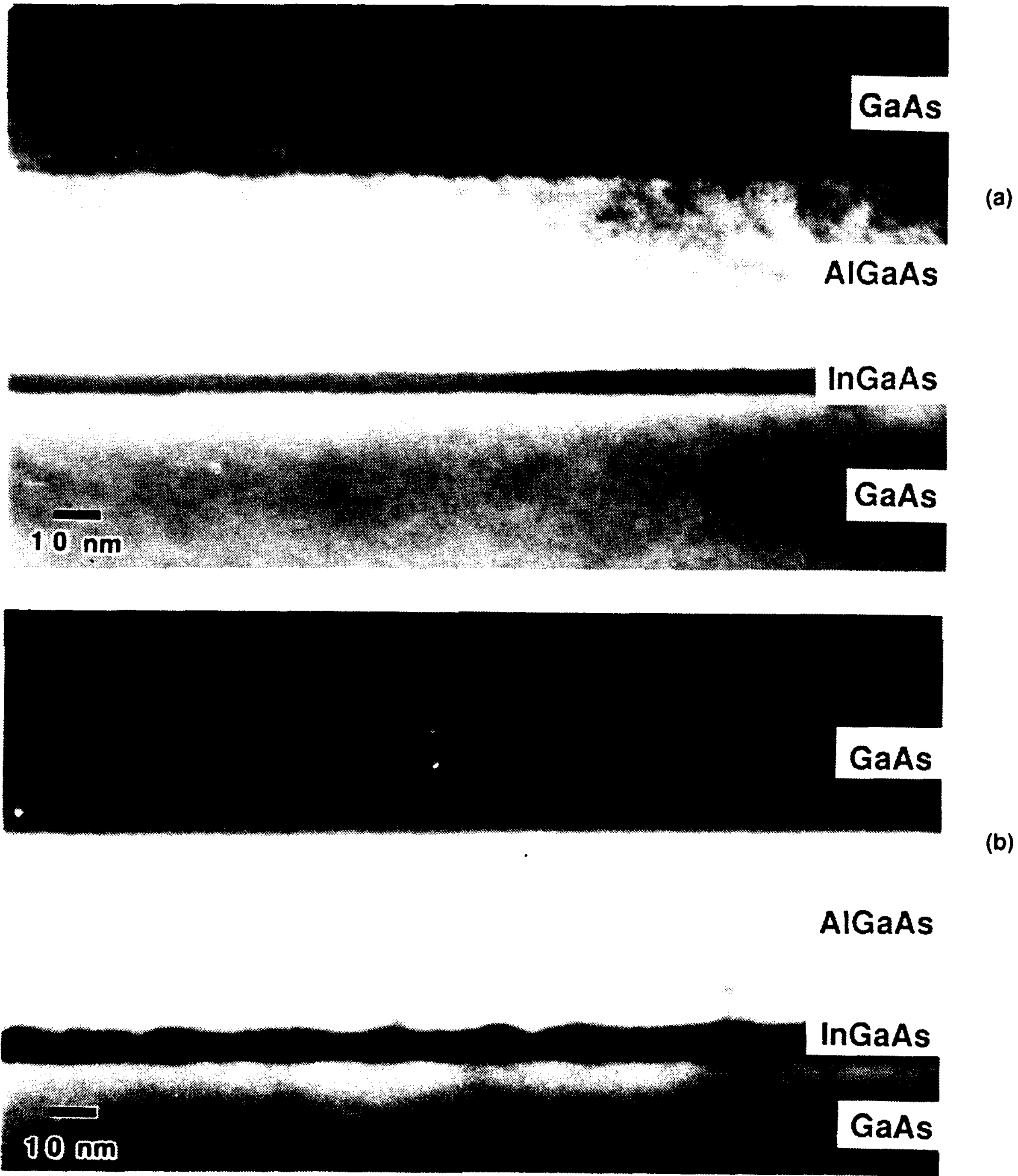

Figure 14. Superlattice Dark Field (110) TEM Cross-sections of (a) x=0.35 (3-534) and (b) x=0.4 (3-665) $In_xGa_{1-x}As$ Single Quantum Well Structures

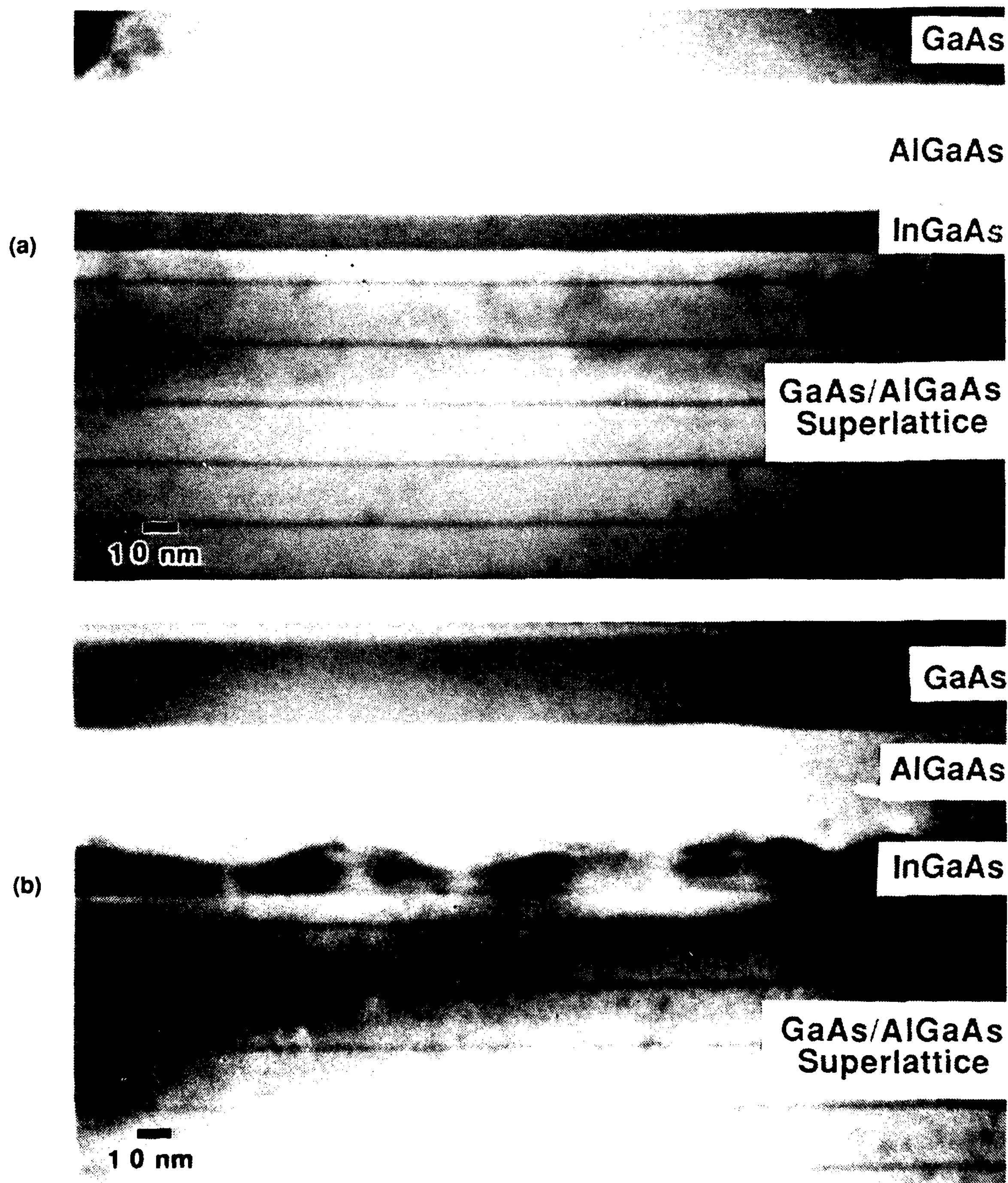

Figure 15. Superlattice Dark Field (110) TEM Cross-Sections of $In_{0.2}Ga_{0.8}As$ Single Quantum Wells Grown on GaAs-AlGaAs Superlattices (SL) with (a) 680°C SL Growth Temperature (3-872) and (b) 520°C SL Growth Temperature (3-873).

growth front becomes deleterious to electron transport. We note here that the "threshold" thickness as described here doesn't necessarily coincide with the dampening of RHEED oscillations or the critical layer thickness as it appears to at higher growth temperatures (>550°C).[16] Again this relates to the non-equilibrium nature of both the growth and dislocation formation at 480°C.

E. Photoluminescence Measurements and Modeling

We performed low temperature photoluminescence on several of the modulation-doped samples grown for this study. Some results are shown in Table 5. In cases where multiple peaks were observed, the principle peak (largest magnitude) is listed in the table. Figure 16 shows representative spectra. Emission from the single quantum well samples tends to show broader peaks closer to the unstrained InGaAs band gap, while the TSSL peaks are sharper and closer to the predicted transition energies. TSSL spectra show a smaller, broader peak in addition to the sharp quantum well peak recorded in Table 5. The broader peaks have been observed elsewhere and have been attributed to impurity or interface states.[17] Previous work at GE has shown that the 2K PL full width at half maximum (FWHM) increases monotonically with the 77K sheet density measured by Hall effect, and that a FWHM of 10-20 meV is typical for a 150Å-thick modulation doped SQW with a sheet density of $2\text{-}3 \times 10^{12}$ cm^{-2}.[18] Generally, the samples with relatively degraded mobilities listed in Tables 3 and 4 also have broader PL FWHM. For example, compare mobility data for the x=0.4 TSSLs (8800 vs 1100 $cm^2/V\text{-}s$) with their PL FWHM (19.3 vs 27.0 meV).

PL transition energies are predicted by a model developed at GE which employs the transfer matrix approach.[19] The conduction, heavy hole and light hole valence bands are modeled separately within an effective mass approximation. The presence of modulated planar doping imposes a considerable electric field on the well, which dictates a solution to Schrodinger's equation based on a linear combination of Airy functions.[20,21] If we subdivide each layer as necessary into several smaller regions, each of which has a uniform electric field, we can approximate the true potential with one for which the exact wave functions can be found. Given the wave func-

Table 5. 2K Photoluminescence Results for GaAs(h_1)-$In_xGa_{1-x}As$(h_2) TSSLs and $In_xGa_{1-x}As$ SQWs

Sample	X	h_1/h_2 (Å)	No. of Periods	Predicted Wavelength (Å)	Observed Wavelength (Å)	FWHM (meV)
3-448	0.30	15/30	3	9326	9348	11.4
3-449	0.30	15/42	3	9483	9875	10.8
3-450	0.30	15/52	3	9663	10055	11.1
3-533	0.30	15/62	2	9601	10170	11.4
3-452	0.35	15/30	3	9505	9900	13.9
3-535	0.35	15/32	2	9133	9712	27.7
3-668	0.40	15/25	2	9092	9460	19.3
3-664	0.40	15/34	2	9473	10060	27.0
3-451	0.30	78	SQW	9203	10430	29.2
3-532	0.30	80	SQW	9225	10490	24.9
3-534	0.35	50	SQW	8980	10500	35.1
3-665	0.40	48	SQW	9199	10860	42.5

R-8/90-5AT

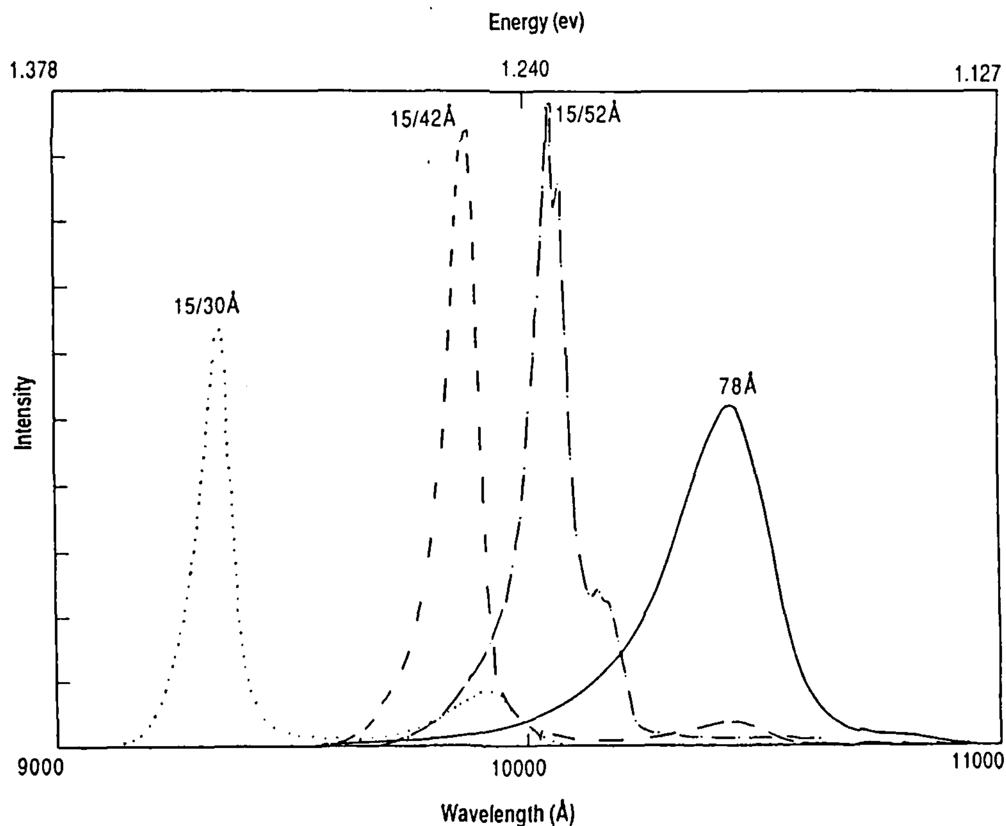

Figure 16. 2K Photoluminescence Scan of Three GaAs(h_1)-$In_{0.3}Ga_{0.7}As$(h_2) TSSLs (h_1=15Å, h_2 = 30, 42, 52Å) and One $In_{0.3}Ga_{0.7}As$(78Å) SQW

tions and the occupation of the various states, one can calculate the electron distribution in the channel and its contribution to Poisson's equation. We thus solve Schrodinger's and Poisson's equations self-consistently to find the energy levels, occupation and distribution of electrons in the conduction band under steady-state conditions. The valence band is modeled in the same way with the exception that no self-consistency is required, as we assume that electrons are the only mobile carriers in the structure present in sufficient quantities to affect Poisson's equation. Exciton binding energies are not calculated or included at this point. We find in general that the field imposed by the planar doping lowers the transition energy due to the effective reduction of the band gap by the voltage drop across the well. This is in spite of the tendency of the field to raise the energy levels in each well.

Table 5 shows good agreement between the predicted and observed PL energies, generally within ~50 meV for the TSSL structures. The wider discrepancy between the predicted and observed values for SQWs is not clear. A sample calculation is shown in Figure 17 for the conduction band of a TSSL structure with three periods of $In_{0.3}Ga_{0.7}As$ (52Å)-GaAs (15Å) with an $Al_{0.3}Ga_{0.7}As$ buffer layer. The $In_{0.3}Ga_{0.7}As$ layers in this case are divided into four sublayers each to approximate a continuously varying electric field. The square of the wave function is plotted for each of three energy levels. The electron spatial density n(x) is also plotted. The model confirms the intuitive result that the TSSL electrons tend to be spatially concentrated in the $In_{0.3}Ga_{0.7}As$ layer closest to the AlGaAs modulation doped layer and have a small probability distribution in the thin GaAs layers of the TSSL.

F. Shubnikov-de Hass Measurements and Modeling

Shubnikov-de Hass (SdH) measurements and numerical determinations of subband occupancies of pseudomorphic TSSL and SQW structures were conducted at Sandia National Laboratories by Chris Tigges, Jim Schirber, and Ian Fritz. The results of transport measurements of the three samples studied to date are given in Table 6. Using a van der Pauw geometry, the mobili-

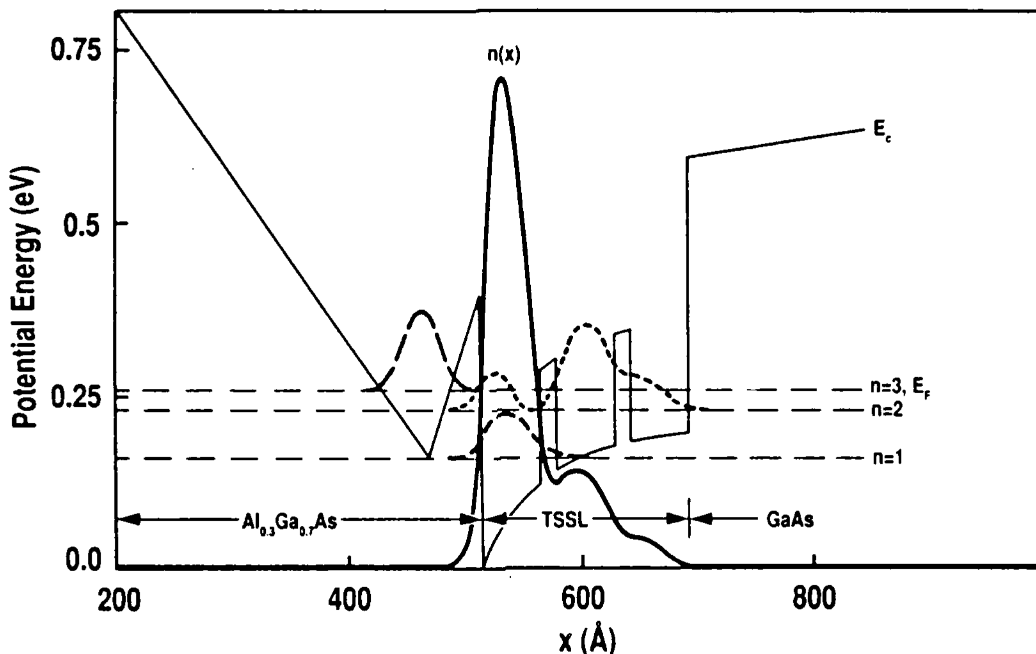

Figure 17. 2K Electron Density n(x) and Electron Wave Function Spatial Distribution and Energy Levels Computed Self-Consistently from Poisson's and Schrodinger's Equations for a Modulation-Doped GaAs(15Å)-$In_{0.3}Ga_{0.7}As$(52Å) Three Period TSSL. (The Fermi level is located just below the n = 3 subband.)

ties (μ) and areal charge densities (N_s) have been determined at 77 and 4K for each of the samples. As can be seen in all cases, both the μ and N_s decrease slightly from 77 to 4K. More interestingly, the SdH oscillations of the two TSSL samples (3-448 and 3-449) have two components with distinct frequencies, while the SQW (3-451) sample's oscillation is composed of a single frequency. In addition, the effective masses determined from the temperature dependence of the oscillation amplitudes, differ significantly among the samples, being somewhat smaller for the TSSLs.

The carrier concentrations derivable from the SdH frequencies agree within combined experimental uncertainties with the transport values. Also, 9% and 18% of the total free charge is associated with the lower frequency respectively for TSSLs 3-448 and 3-449. The temperature dependent amplitudes of both components of the 3-449 oscillations could be determined giving the same effective mass to within error limits.

Table 6. Shubnikov-de Hass and van der Pauw Measurement Results

Sample	h_1/h_2 (Å)	No. of Periods	77 K Mobility	77 K Sheet Density	4 K Mobility	4 K Sheet Density
3-448	15/30	3	12,700	2.5×10^{12}	12,600	2.32×10^{12}
3-449	15/42	3	10,300	2.6×10^{12}	9,600	2.59×10^{12}
3-451	78	SQW	14,500	3.0×10^{12}	11,700	3.78×10^{12}

R-8/90-6AT

Numerical determinations of the static conduction electronic structure have been made using a self-consistent Schrodinger-Poisson algorithm in the Hartree approximation. The charge neutral band structure and zone center effective masses including alloy and strain effects is determined using elastic constants and deformation potentials. From this a 1D finite element mesh is developed fully describing the band structure, effective mass, doping concentration, dopant band offset, and permittivity with respect to the mesh. Then the one dimensional effective mass Schrodinger equation can be cast using a finite element technique (Galerkin residual method) into a symmetric tridiagonal matrix formulation of the generalized eigenvalue problem. Any and particularly the low lying eigenvalues and eigenvectors are determined using a generalized inverse power iteration method. The occupancy of the eigenstate is determined using Fermi Dirac statistics and a 2D density of states for the lowest lying states, while the upper states are combined approximately by crossing over to a 3D density of states. The 1D Poisson equation is then solved analytically using the charge distribution generated by the previous stage. The resulting electronic potential modifies the effective potential of the Schrodinger equation establishing self-inconsistency. The whole system is then relaxed to numerical self-consistency iteratively with surface charge control pinning the Fermi level as desired and the remaining charge distributed appropriately between the donors and the conduction band.

Many-body effects such as band gap narrowing associated with exchange and correlation of the carriers and ionized donor-donor interactions can be treated approximately by modifying the effective potential in the Schrodinger equation (for example using a local density approxima-

tion). However, the carrier-carrier and ionized donor-donor interactions compensate one another to a great extent as far as the relative position of energy levels to the Fermi level is concerned and consequently, these interactions do not greatly affect the overall charge control problem. Therefore, we did not include any approximations for many-body effects in the present calculations. An additional complication is created by the variation of the longitudinal effective mass along the z axis, especially at the $Al_{0.3}Ga_{0.7}As/In_{0.3}Ga_{0.7}As$ interface, inducing nonparabolicity into the transverse dispersion relation. Although this effect can be incorporated numerically through a transverse k dependent effective potential, the effect is expected to be negligible for the lowest energy states (recall the equivalence of the SdH derived m* values for 3-449), and as a result we used the 2D density of states determined by the effective mass derived for the $In_{0.3}Ga_{0.7}As$ alloy layer.

We determined the static electronic band structure and low lying quantum states at 4K for each of the structures to compare with the low temperature SdH measurements. The resulting conduction band profiles and low lying energy levels are shown consecutively in Figures 18-20. The form of the low lying wave functions are superposed on the energy levels. Dramatic differences exist for the envelope wave functions between the ground state subband, localized to a great extent in the InGaAs layer of the first period, and the first excited state subband which is localized to a lesser extent in the InGaAs layer of the third period for the TSSLs. At 4K only the first two subbands of the TSSLs and the ground state subband of the SQW are occupied at a level accessible to the SdH technique. Moreover, the total free charge and areal charge density ratios are consistent with the SdH results. In fact there is excellent agreement between the measured and calculated occupation ratios (See Table 7). One might expect that the total free charge and, therefore, the subband occupations are more sensitive to inaccuracies in determining the modeling parameters such as the effective masses and Fermi pinning level than are the occupation ratios. Nevertheless, these preliminary results are very encouraging.

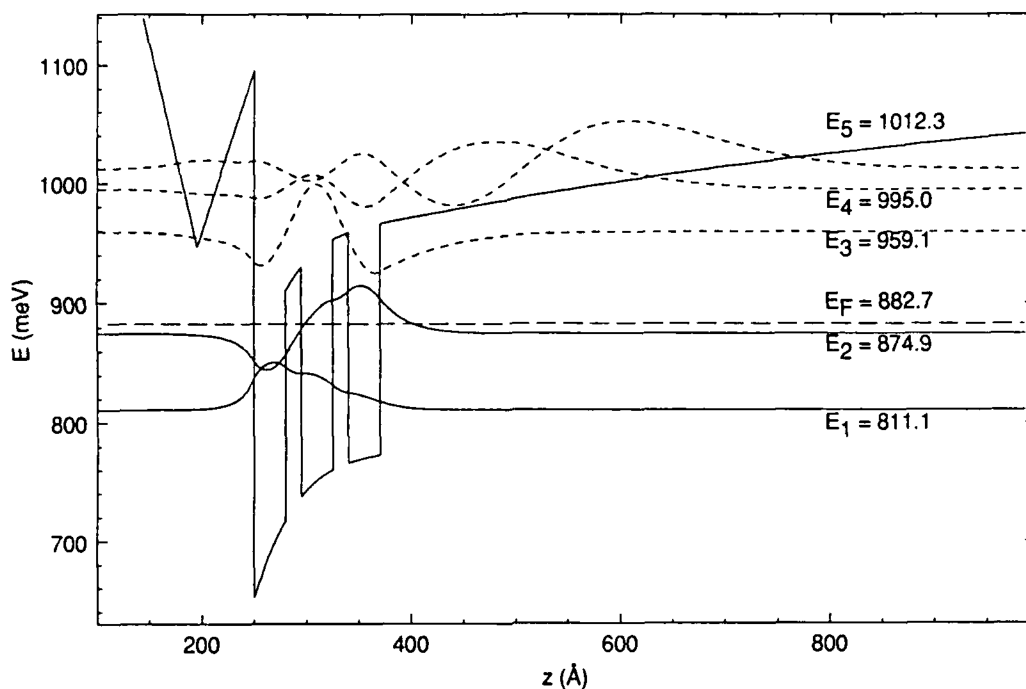

Figure 18. Self-Consistent Calculation for Conduction Band Profile, Energy Levels, and Wave Functions for GaAs(15Å)-$In_{0.3}Ga_{0.7}As$ (30Å) TSSL (3-448)

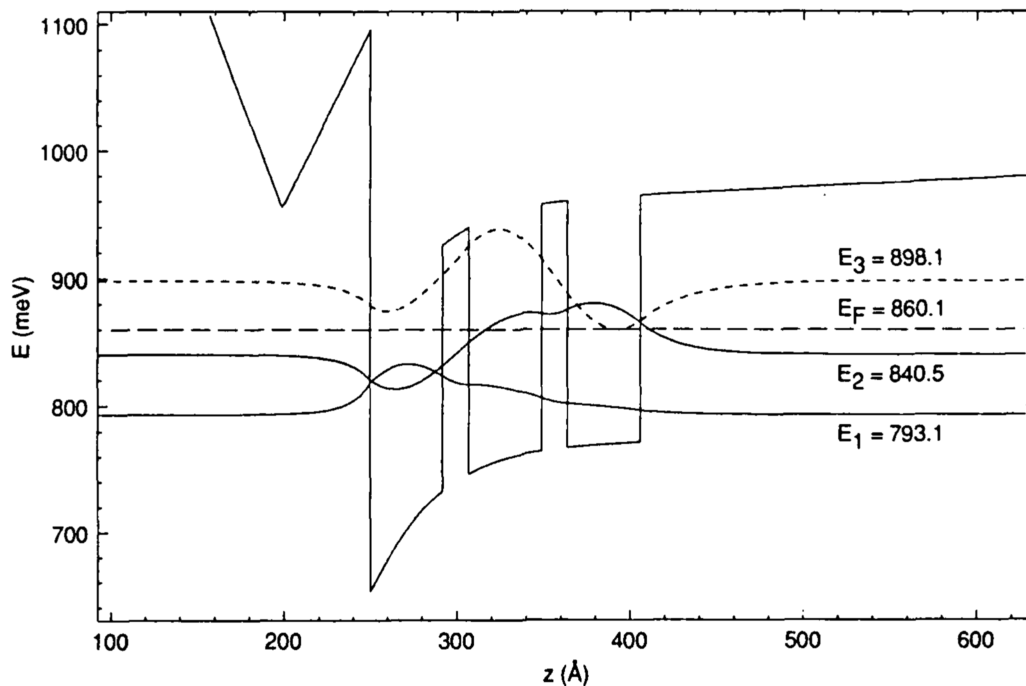

Figure 19. Self-Consistent Calculation for Conduction Band Profile, Energy Levels, and Wave Functions for GaAs (15Å)-$In_{0.3}Ga_{0.7}As$ (42Å) TSSL (3-449)

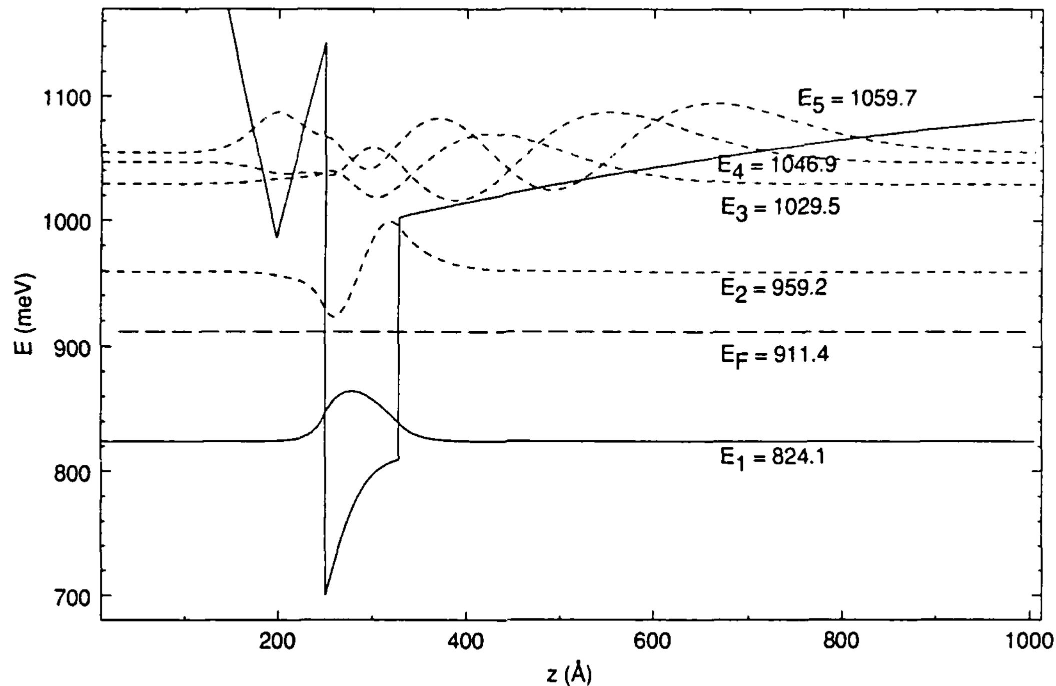

Figure 20. Self-Consistent Calculations for Conduction Band Profile, Energy Levels, and Wave Functions for $In_{0.3}Ga_{0.7}As$ (78Å) SQW (3-451)

In summary, we observe SdH oscillations composed of two frequencies for the TSSL structures studied and of one frequency for the SQW structure studied. These observations have been shown to correspond with the occupation, at low temperatures, of the first two conduction subbands in the TSSL structures and only the first subband in the SQW structures as determined by numerical simulations of the static electronic profiles. The subband occupation ratios of the TSSLs as determined by the SdH measurements and the numerical results are nearly identical, and the total free charge densities are comparable. In light of this correspondence, neglecting many-body interactions and subband dispersion details appears to have been justified. Despite these apparent consistencies, the effective masses derived from the SdH results vary significantly and unexpectedly between the different structures. These variations, though as yet unexplained, are intriguing and remain the subject of further investigation.

Table 7. Comparison of SdH and Numerical Subband Occupations (percent total free charge)

Sample	h_1/h_2 (Å)	No. of Periods	SdH frequencies		Numerical Subbands	
			High	Low	Ground	Excited
3-448	15/30	3	91	9	90	10
3-449	15/42	3	82	18	79.8	20.2
3-451	78	SQW	100	0	100	0

R-8/90-7AT

G. Photoreflectance Measurements and Franz-Keldysh Oscillations

Photoreflectance (PR) measurements were conducted by Prof. Fred Pollak at Brooklyn College. Photoreflectance is contactless and non-destructive. Modulated illumination of an isolated quantum well, with above band-gap light (pump beam) is known to yield a first derivative spectroscopy in the dielectric function. The experimental set-up used at Brooklyn College is shown in Figure 21. Previous PR measurements of samples with 2-DEGs[22-24] have noted Franz-Keldysh oscillations in the above band gap reflectance, but it hasn't been shown conclusively that the oscillations are actually due to a modulation of the quantized system itself. For example, Bernussi, et.al.,[24] investigated modulation doped AlGaAs-GaAs and δ-doped GaAs samples. Through detailed temperature dependent and intensity dependent measurements, they concluded that the oscillations they observe are due to changes in the built-in fields in regions close to the capping layer for the δ-doped sample and in the buffer layer for the modulation-doped sample.

For the samples studied here, we have observed strong Franz-Keldysh oscillations which we can conclusively relate to the quantized pseudomorphic InGaAs. Figure 22 shows PR spectra for two different modulation doped pseudomorphic structures.

Layer 3-1043 has the InGaAs layer grown by MBE/MEE at 300°C while that of sample 3-1044 is grown by conventional MBE at 300°C. The growth conditions are discussed in Section A, and a representative TEM cross-section of the samples is shown in Figure 2. The PR features are more pronounced and somewhat sharper for layer 3-1043, correlating with the electron

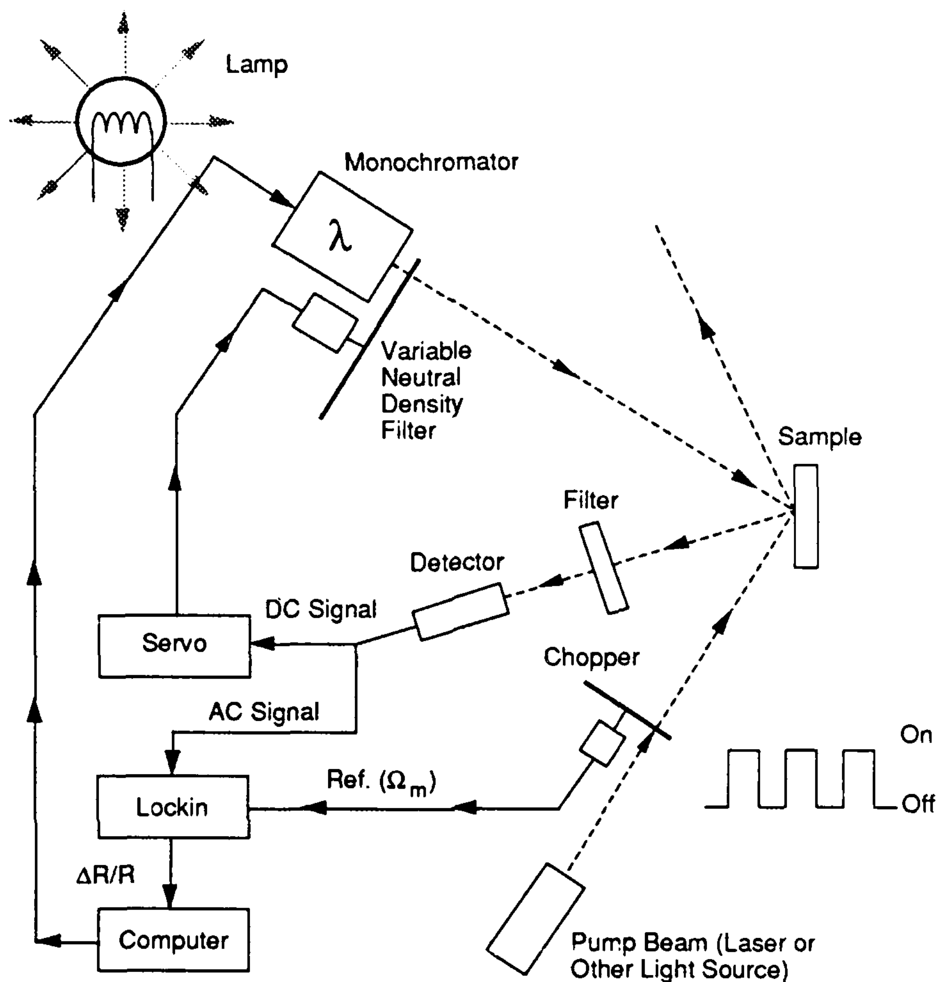

Figure 21. Schematic Representation of the Brooklyn College Photoreflectance Apparatus

mobility data noted in Section A. Both samples exhibit Franz-Keldysh oscillations, with the maxima and minima denoted in the case of 3-1043. The identification as Franz-Keldysh oscillations is shown in Figure 23 by the linear relationship between index number and $(E_n\text{-}E_g)^{3/2}$, where E_n is the energy associated with the nth maxima or minima in the PR spectrum and E_g is the band gap. Since the oscillations occur well below the band gap of the GaAs or AlGaAs layers in the heterostructure, it is unambiguous to ascribe the Franz-Keldysh oscillations to the pseudomorphic InGaAs. This is the first time that Franz-Keldysh oscillations have been clearly attributed to

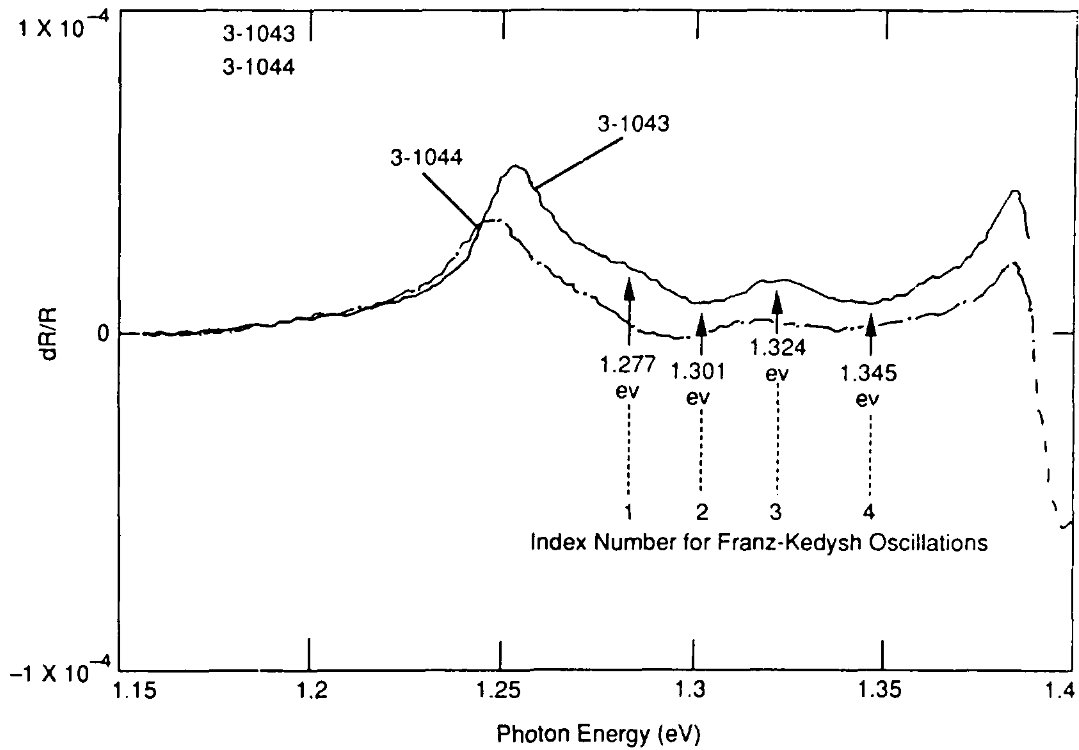

Figure 22. Room Temperature Photoreflectance of MBE (3-1044) and MBE/MEE (3-1043) Modulation-Doped Pseudomorphic $In_{0.2}Ga_{0.8}As$ Structures Grown at 300°C

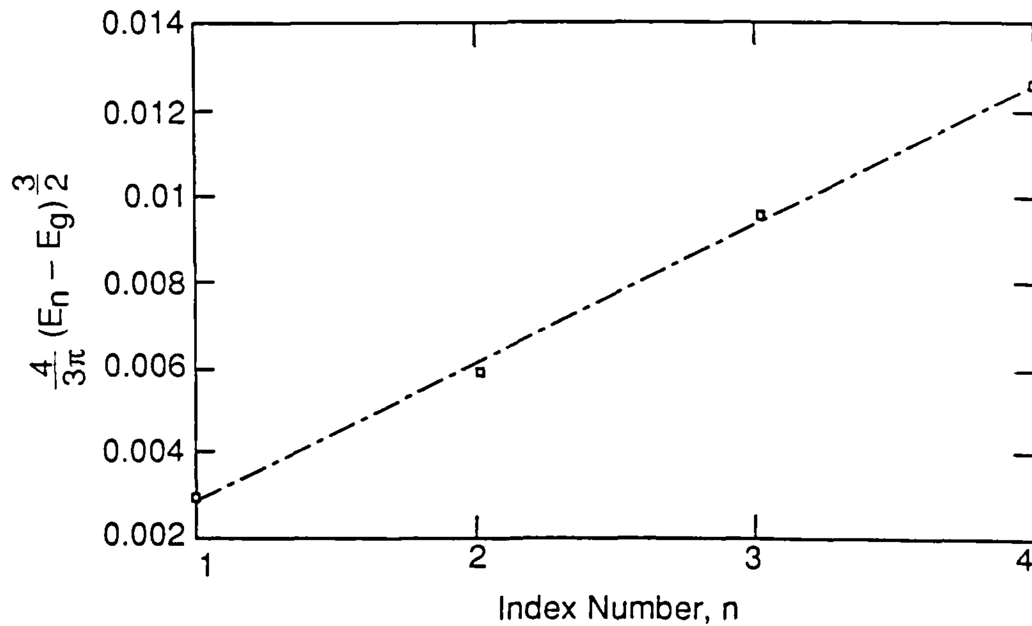

Figure 23. Plot of Energy Dependence for Franz-Keldysh Oscillations (n=1,2,3,4) Noted in Figure 22 for Sample 3-1043

a quantized system. It may be possible in the future with modeling to relate the oscillations to physical parameters such as 2-DEG density.

H. Microwave Reflectance Measurements

Microwave reflectance measurements were performed by J. Singh and J.M. Borrego at Rensselaer Polytechnic Institute. The technique has potential as a non-contacting measurement of pseudomorphic HEMT 2-DEG densities and mobilities. The apparatus used is shown in Figure 24.

Electron mobilities were obtained for both front and backside illumination with the laser and microwave, by applying a DC magnetic field transverse to the microwave electric field. A decrease in photoconductivity (PC) is observed when the DC magnetic field is applied due to the magneto-resistance effect. The relationship between the mobility and the change in PC is:

$$\frac{\Delta\sigma}{\sigma} = \mu^2 B^2 T_M \qquad (2)$$

where T_M is the magneto-resistance coefficient. Thus, the change in PC should be linear with respect to B^2, and this was indeed observed during the experiments.

Room temperature PC transients (front⇔heterolayer side, and back⇔SI-GaAs side) were measured for three samples (3-1043, 3-1044 and 3-1046) and 77K transients were measured for one sample. A large PC response is obtained for the case of zero magnetic field and a smaller response is obtained with a 5kG DC magnetic field applied. The wavelength used was 904nm, which is below bandgap for both GaAs and AlGaAs, but above bandgap for InGaAs. Table 8 shows the mobility calculated from the change in peak photoconductivity. For this case, the appropriate contacting Hall effect results are for the sample after all of the n^+ GaAs and some of the n AlGaAs is removed. As mentioned earlier in this report, we step etch the samples until we achieve the peak in the 77K mobility. This has given us good agreement with Shubnikov-de Hass oscillations for 2-DEG properties, so we are confident that the μ_{Hall} data in Table 8 is due

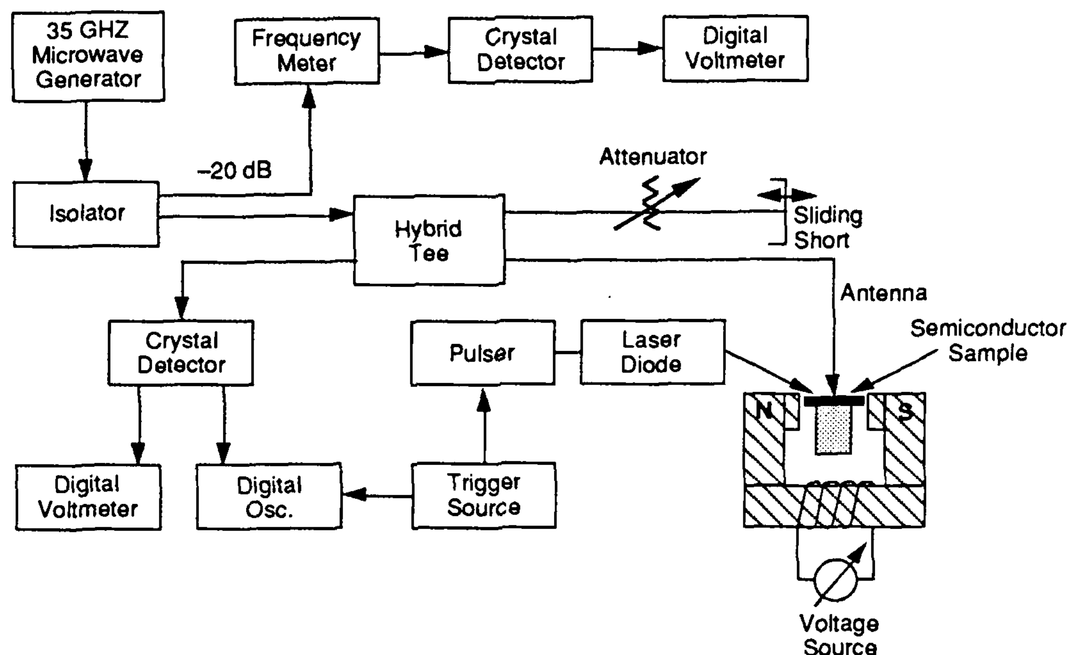

Figure 24. Schematic Representation of the Rensselaer Polytechnic Institute Microwave Reflection Measurement System

only to the 2-DEG in the InGaAs. Sample 3-1044 has the lowest mobility, while 3-1043 has the highest mobility. This trend correlates with the relative magnitudes, assessed by contacting Hall effect measurements, but the data is complicated by the GaAs substrate.

Bare SI GaAs substrates examined by this technique exhibit μ_{300K} ~6000 cm²/V-s and μ_{77} ~14,000 cm²/V-s, very similar to the InGaAs 2-DEG Hall effect mobilities. We presume EL2 in the SI GaAs to have an absorption coefficient for 904nm of ~1 cm^{-1} and the InGaAs quantum wells to have an absorption coefficient of ~10^4 cm^{-1}. Given their relative thicknesses (100Å vs. 500μm), their absorption and resulting PC would then be of the same order.

With the laser off, and thus not exciting EL2, we performed microwave reflectance. Unfortunately, this doesn't selectively sample the InGaAs, but measures the sheet resistivity for the entire structure (n^+ GaAs cap, n AlGaAs, and InGaAs). Results are shown in Table 9. The mobility (μ_{MR}) is calculated from the measured sheet resistivity (ρ_{MR}) assuming an electron sheet

Table 8. Comparison of Photo-Induced Microwave Reflectance and Hall Effect

		300K $\mu T_M^{1/2}$ (cm^2/V-s)	300K μ_{Hall} (cm^2/V-s)	77K $\mu T_M^{1/2}$ (cm^2/V-s)	77K μ_{Hall} (cm^2/V-s)
3-1043	(front)	6100	5380	—	—
	(back)	6000			
3-1044	(front)	5000	2000	—	—
	(back)	5500			
3-1046	(front)	5600	5370	—	14,000
	(back)	5800		14,000	

R-8/90-8AT

Table 9. 77K Comparison of Microwave Reflectance (no laser) and Hall Effect for As-Grown Layer (GaAs-AlGaAs-InGaAs)

	ρ_{MR}	μ_{MR}	ρ_{Hall}	μ_{Hall}
3-1046	120 Ω/□	10,400 cm^2/V-s	117 Ω/□	10,930 cm^2/V-s

R-8/90-9AT

density of 5.0×10^{12} cm^{-2}, which is what contacting Hall measurements yielded on the as-grown unetched structure. Excellent agreement was achieved at 77K. While this technique is not truly selective for the InGaAs, it is somewhat selective since the InGaAs 2-DEG dominates the conductivity of the GaAs-AlGaAs-InGaAs structure, especially so at 77K. To conclude, the technique appears at this preliminary stage to have utility for measurements on pseudomorphic HEMTs. More samples are being evaluated.

I. References

1. P.L. Gourley, I.J. Fritz, and L.R. Dawson, *Appl. Phys. Lett.*, 52, 377 (1988).
2. G.J. Whaley and P.I. Cohen, *J. Vac. Sci. Technol.* B6, 625 (1988).
3. D.C. Radulescu, W.J. Schaff, L.F. Eastman, J.M. Ballingall, G.O. Ramseyer, and S.D. Hersee, *J. Vac. Sci. Technol.* B7, 111 (1989).
4. Z. Liliental-Weber, F. Smith, and A.R. Calawa, Materials Research Society Spring Meeting, San Francisco, Ca, April 16-20, 1990, and Workshop on Low Temperature GaAs Buffer Layers, San Francisco, CA, April 20, 1990.
5. M.R. Melloch, Workshop on Low Temperature GaAs Buffer Layers, San Francisco, CA, April 20, 1990.
6. J.M. Ballingall, Workshop on Low Temperature GaAs Buffer Layers, San Francisco, CA, April 20, 1990.
7. P.S. Peercy, B.W. Dodson, J.Y. Tsao, E.D. Jones, D.R. Myers, T.E. Zipperian, L.R. Dawson, R.M. Biefeld, J.F. Klem, and C.R. Hills, *IEEE Electron Device Lett.* EDL-9, 621 (1988).
8. P.C. Chao, P. Ho, K. Duh, P. Smith, J. Ballingall, A. Jabra, *Electronic Lett.* 26, 27 (1990).
9. A. Fischer-Colbrie, J.N. Miller, S.S. Laderman, S.J. Rosner, and R. Hull, *J. Vac. Sci. Technol.* B6, 620 (1988).
10. T. Henderson, M. Aksun, C. Peng, H. Morcoc, P.C. Chao, P.M. Smith, K.H.G. Duh, and L.F. Lester, *IEEE Electron Device Lett.* EDL-7, 645 (1986).
11. G.C. Osbourn, *J. Vac. Sci. Technol.* B1, 379 (1983).
12. S.V. Ghaias and A. Madhukar, *Appl. Phys. Lett.* 53, 1599 (1988).
13. B.F. Lewis, T.C. Lee, F.J. Grunthaner, A. Madhukar, R. Fernandez, and J. Maserjian, *J. Vac. Sci. Technol.* B2, 419 (1984).

14. P.R. Berger, K. Chang, P.K. Bhattacharya, and J. Singh, *J. Vac. Sci. Technol.* B5, 1162 (1987).

15. P.G. Newman, M.M. Cho, D.J. Kim, A. Madhukar, D.D. Smith, T.R. Aucoin, and G.J. Iafrate, *J. Vac. Sci. Technol.* B6, 1483 (1988).

16. B. Elman, E.S. Koteles, P. Melman, C. Jagannath, J. Lee, and D. Dugger, *Appl. Phys. Lett.* 55, 1659 (1989).

17. N.G. Anderson, W.D. Ladig, R.M. Kolbas and Y.C. Lo, *J. of Appl. Physics* 60, 2361 (1980).

18. B.R. Lee, G.J. Tessmer, P.A. Martin, T.H. Yu, and J.M. Ballingall, 1987 Electronic Materials Conference, Santa Barbara, CA (June, 1987).

19. R. M. Kolbas and N. Holonyak, Jr., *Am. J. Phys.* 52, 431 (1984)

20. Wayne W. Lui and Masao Fukuma, *J. Appl. Phys.* 60, 155 (1986).

21. K.F. Brennan and C.J. Summers, *J. Appl. Phys.* 61, 614 (1987).

22. O.J. Glembocki, B.V. Shanabrook, N. Bottka, W.T. Beard and J. Comas, *Appl. Phys. Lett.* 46, 970 (1985); also *Proc. SPIE* 524, 86 (1985).

23. E.S. Snow, O.J. Glembocki and B.V. Shanabrook, *Phys. Rev.* B38, 12483 (1988).

24. A. Bernussi, C.A.C. Mendonca, P. Motisuke, E.A. Meneses, F. Cerdeira, F.H. Pollak, P. Basmaji and I.F.L. Dias, to be published in the Proceedings of the 20th Int. Conf. on the Physics of Semiconductors, Thessaloniki, 1990.

III. SUGGESTIONS FOR FUTURE WORK

There have been a limited number of growth studies of pseudomorphic InGaAs by techniques other than MBE. Growth of pseudomorphic InGaAs by MOVPE and MOMBE in the MEE and ALE modes of growth would be an interesting comparison to the MBE and MBE/MEE results. Because of the high surface mobility of MO species, it's possible that low temperature grown structures could have a superior quality to their MBE counterparts, forestalling island growth to lower temperatures.

Low temperature MBE/MEE growth of entire pseudomorphic device structures would likely foster major breakthroughs in terms of what compositions could in practice be used successfully on a GaAs or InP substrate. We demonstrated 300°C MBE/MEE quantum wells to have very good 2-DEG properties, but noted that the overlayers of AlGaAs which contribute modulation doping generally need to be grown above 450°C, countering the benefits of 300°C growth in terms of circumventing dislocation formation and extending the critical composition/layer thickness. Development of growth technology to provide conducting layers of AlGaAs and GaAs at 300°C is needed to exploit the MBE/MEE InGaAs 300°C results. The variation of effective mass between x=0.3 single quantum well and thin strained superlattices which was observed in the present work, is an intriguing result with obvious potential benefits for high speed devices. Evaluation of additional samples and modeling would be useful.

Further work could be well spent in developing the contactless non-destructive assessment techniques described in this report. Photoluminescence, photoreflectance, and microwave reflectance have great potential to provide details on pseudomorphic InGaAs heterostructure quality and 2-DEG electronic properties. It's clear that pseudomorphic InGaAs heterostructure devices will play a major role in GaAs-based MMICs and discrete devices for microwave and millimeter wave applications in the 1990's. Techniques for evaluating/screening 3-inch wafers for device processing will be indispensable.

IV. PUBLICATIONS

- "Novel Pseudomorphic High Electron Mobility Transistor Structures with GaAs-$In_{0.3}Ga_{0.7}As$ Thin Strained Superlattice Active Layers," J.M. Ballingall, P. Ho, G.J. Tessmer, P.A. Martin, Nathan Lewis, and Ernest L. Hall, *Applied Physic Letters* 54, 2121 (1989).
- "Materials Characteristics of Pseudomorphic High Electron Mobility Transistor Structures with GaAs-$In_xGa_{1-x}As$ ($0.25< x <0.4$) Thin Strained Superlattice Active Layers," J.M. Ballingall, P. Ho, P.A. Martin, G.J. Tessmer, T.H. Yu, Nathan Lewis, Ernest Hall, *Journal of Electronic Materials* 19, 509 (1990).
- "Materials and Device Characteristics of Pseudomorphic AlGaAs-InGaAs-GaAs and AlInAs-InGaAs-InP High Electron Mobility Transistors," J.M. Ballingall, Pin Ho, G.J. Tessmer, P.A. Martin, T.H. Yu, P.C. Chao, P.M. Smith, and K.H.G. Duh, Proceedings of the Materials Research Society, Symposium D: Layered Structures, Fall 1989 Meeting, Boston, MA.
- "Very Low Noise $Al_{0.3}Ga_{0.7}As/Ga_{0.65}In_{0.35}As$/GaAs Single Quantum Well Pseudomorphic HEMTs," P.C. Chao, P. Ho, K. Duh, P. Smith, J. Ballingall, A. Jabra, *Electronic Lett.* 26, 27 (1990).

The following publications are currently in preparation:

- "Subband Occupation and Effective Masses of $In_{0.3}Ga_{0.7}As$/GaAs Thin Strained Layer Superlattice Structures," C.P. Tigges, J.E. Schirber, I.J. Fritz, Pin Ho, P.A. Martin and J.M. Ballingall.
- "Improved Device Performance by Migration-Enhanced Epitaxy," Pin Ho, S.C. Wang, T.H. Yu, J.M. Ballingall, S.M.J. Liu and K.H.G. Duh.
- "Low Temperature (300°C) $In_{0.3}Ga_{0.7}As$ Electrical and Structural Properties," J.M. Ballingall, Pin Ho, G. Hutchins, and E. Hall.
- "Franz-Keldysh Oscillations in Modulation-doped AlGaAs-InGaAs-GaAs Structures," F.H. Pollak, P. Ho, P. Martin, J.M. Ballingall.
- "Electronic Properties of Pseudomorphic HEMT Structures Measured by Microwav Reflectance," K. Singh, J.M. Borrego, P. Ho, J.M. Ballingall.

V. PRESENTATIONS

- "Materials Characteristics of Pseudomorphic High Electron Mobility Transistor Structures with GaAs $In_xGa_{1-x}As$ ($0.25< x <0.4$) Thin Strained Superlattice Active Layer," J.M. Ballingall, P. Ho, P.A. Martin, G.J. Tessmer, T.H. Yu, Nathan Lewis, Ernest Hall, 1989 Electronic Materials Conference, Cambridge, MA.
- "Materials and Device Characteristics of Pseudomorphic AlGaAs-InGaAs-GaAs and AlInAs-InGaAs-InP High Electron Mobility Transistors," J.M. Ballingall, Pin Ho, G.J. Tessmer, P.A. Martin, T.H. Yu, P.C. Chao, P.M. Smith, and K.H.G. Duh, Materials Research Society, Symposium D: Layered Structures, Fall 1989 Meeting, Boston, MA, November, 1989 (INVITED).
- "The Inverted Interface Problem and Electron Transport in Modulation-Doped AlGaAs-GaAs-AlGaAs and AlGaAs-InGaAs-AlGaAs Heterostructures," P. Ho, G. Tessmer, B. Lee, P. Martin, J.M. Ballingall, N. Lewis, E.L. Hall, 10th Workshop for Molecular Beam Epitaxy, Raleigh, NC, September 1989.
- "Improved Device Performance by Migration Enhanced Epitaxy," P. Ho, S. Wang, T. Yu, J.M. Ballingall, S.M.J. Liu, and K.H.G. Duh, International Conference on Molecular Beam Epitaxy, LaJolla, CA, August, 1990.

VI. PROFESSIONAL RESEARCH PERSONNEL

1. Dr. James M. Ballingall, Principal Investigator
   Manager, Epitaxial Technology

2. Dr. Pin Ho
   Senior Materials Engineer

3. Dr. Tan-hua Yu
   Manager, Prototype Devices

4. Dr. Paul A. Martin
   Materials Engineer

5. Dr. Ernest L. Hall
   Supervisor, Analytical Electron Microscopy

6. Mr. Nathan Lewis
   Materials Engineer

7. Mr. Glenn J. Tessmer
   Materials Engineer

8. Mrs. Gudrun Hutchins
   Materials Engineer